Broadband sensitizers for erbium-doped planar optical amplifiers: review

Albert Polman

FOM–Institute for Atomic and Molecular Physics, Kruislaan 407, 1098 SJ Amsterdam, The Netherlands

Frank C. J. M. van Veggel*

MESA$^+$ Institute, University of Twente, P.O. Box 217, 7500 AE Enschede, The Netherlands

Received July 18, 2003; revised manuscript received December 11, 2003; accepted December 18, 2003

Three different broadband sensitization concepts for optically active erbium ions are reviewed: 1) silicon nanocrystals, with absorption over the full visible spectrum, efficiently couple their excitonic energy to Er^{3+}, 2) silver-related defect states in sodalime silicate glass have absorption in the blue and transfer energy to Er^{3+}, and 3) organic cage complexes coordinated with well-chosen chromophores serve as broadband sensitizers in the visible. Energy transfer rates, efficiencies, and limiting factors are addressed for each of these sensitizers. Implications of the use of strong sensitizers for planar waveguide design are illustrated by using a model for the sensitizing effect of ytterbium. © 2004 Optical Society of America

OCIS code: 060.0060.

1. INTRODUCTION

A. Erbium-Doped Planar Amplifiers

Er-doped materials are of great interest in optical communications technology, as they can serve as the gain medium in lasers and optical amplifiers operating at the standard telecommunications wavelength of 1.5 μm.[1,2] Er^{3+} ions, when incorporated in a solid host, show well-defined energy levels of the 4*f*-shell electronic configurations (see Fig. 1).[3] The transition from the first excited state to the ground state ($^4I_{13/2} \rightarrow {}^4I_{15/2}$) occurs at 1.53 μm and is being employed to provide the gain in optical fiber amplifiers in long-distance telecommunication links worldwide. Currently, planar photonic integrated circuits are being developed to perform functions such as guiding, splitting, switching, wavelength multiplexing, and amplification of light on a single chip. The planar amplifier is an important component in planar integrated photonic circuits. It can serve, e.g., to compensate for coupling losses, waveguide losses, or the power division in optical splitters.

A schematic layout of an Er-doped planar optical amplifier is shown in Fig. 2. Pump and signal beams are coupled into the device through separate input waveguides, and then combined in a wavelength division multiplexer (WDM). Next, an Er-doped waveguide section is rolled up on a small area in the spiral structure (amplifying waveguide spiral, AMP) to combine long interaction length with small device area. After the AMP section, signal and pump are separated in a WDM and a 1×4 splitter is added. The full device would then operate as a loss-free optical splitter. Note that the total device area is determined mostly by the size of the AMP spiral. By using a high-index waveguide core, waveguide bends as small as 50 μm can be made and the spiral dimensions kept as small as 1 mm^2.

We have fabricated an Er-doped amplifier based on Al_2O_3 waveguide technology.[4] To make these waveguides, a SiO_2 buffer layer is first grown on a Si substrate. Next, a 600-nm-thick Al_2O_3 film is deposited by radio frequency magnetron sputtering from an Al_2O_3 target.[5] Er ions are then introduced into the film using ion implantation, and the waveguide layout (as in Fig. 2) is defined by Ar-atom-beam etching. Finally, a SiO_2 cladding layer is deposited, and the input and output facets are mechanically polished. Figure 3 shows an optical gain measurement on this structure in which a 4-cm-long waveguide was doped with Er to a peak concentration of 0.3 at.%. By using 10 mW of laser power at 1.48 μm coupled into the waveguide, a gain at 1.53 μm of 4.0 dB is realized. After subtracting the waveguide loss for this particular waveguide, the net gain (from input to output facet) is 2.3 dB. As far as we know, this is the smallest Er-doped optical amplifier fabricated to date. Several other groups have reported the fabrication of planar optical amplifiers based on silicate glasses.[6–8]

B. Two Major Gain-Limiting Factors

In Fig. 3, the measured pump power dependence of the optical gain was quite different from that predicted from the simple quasi-three-level scheme in Fig. 1, as indicated by the curved dashed line in Fig. 3. The reason is the occurrence of a nonlinear process known as cooperative upconversion that significantly reduces the degree of Er population in the first excited state ($^4I_{13/2}$) at a given pump power.[9] In this process, two excited Er ions exchange energy through a dipole–dipole interaction. As a result, one ion becomes de-excited to the ground state, while another one is excited to the $^4I_{9/2}$ level.

Upconversion is the main gain-limiting factor in planar optical amplifiers. To achieve high gain per unit length,

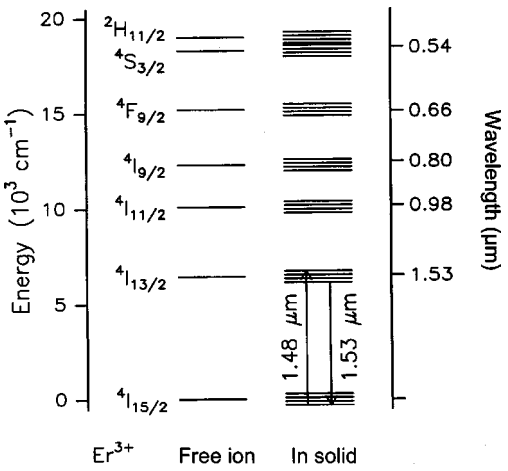

Fig. 1. Energy level diagram of Er^{3+}.

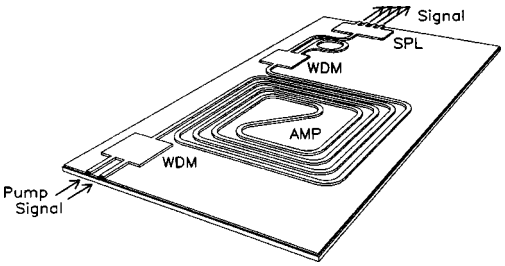

Fig. 2. Schematic of a miniature optical waveguide amplifier. An amplifying waveguide spiral (AMP) is integrated with wavelength division multiplexers (WDM) for pump and signal and a 1×4 splitter (SPL).

a high Er concentration is required. At the same time, for a high Er concentration, cooperative upconversion will cause the effective decay rate from the first excited state to increase, and a higher pump power is required to achieve a certain degree of population inversion. For example, in Fig. 3, the pump power (in the waveguide) required to achieve net gain is 3 mW, while only 0.5 mW would be required if no upconversion took place.

An additional gain-limiting factor in Er-doped amplifiers is excited-state absorption (ESA), which occurs at high pump power. For example, a 1.48-μm pump photon can bring an excited Er ion from the $^4I_{13/2}$ level into the $^4I_{9/2}$ level. The effect of ESA on the optical gain becomes significant when the higher-lying states have appreciable lifetimes, leading to population buildup in levels that do not contribute to gain. ESA becomes important when high pump powers are required, for example, to compensate for the effect of upconversion. The effect of ESA is illustrated in Fig. 4(a), which shows a calculation of the Er population in a waveguide core consisting of a 2-μm wide, 520-nm thick ridge etched into an 800-nm thick, Er-doped Al_2O_3 film.[10] The waveguide is pumped at 1.48 μm at a power of 100 mW. The Er population is plotted as integrated over the thickness of the waveguide. The calculation takes into account the measured upconversion coefficient and Er absorption and emission cross sections, as well as the three-dimensional, 1.48-μm pump and 1.53-μm signal mode distributions. The dip in the center of the waveguide at the entrance facet is due to ESA. The effect on the differential signal gain is seen in Fig. 4(b). It shows that at a pump power of 100 mW, ESA causes net signal loss. As the pump power decreases along the waveguide as a result of both absorption by Er and waveguide losses, the effect of ESA decreases and, initially, the differential gain increases. The differential gain becomes negative near the end of the waveguide because of the reduced pump intensity. The existence of an upper limit on the pump power shows that ESA puts a maximum to the length of a single-end-pumped waveguide amplifier. We note that the ESA cross section is strongly materials dependent, its being relatively large for Al_2O_3 (with widely spread Stark levels) and small for, e.g., silica-based glasses. In addition, the shorter Er^{3+} excited-state lifetimes in silica glasses result in the effect of ESA on the population distribution being smaller in these materials.

As shown above, cooperative upconversion and ESA are the two main factors that determine amplification performance.[11] The strength of both processes determines the optimum concentration, maximum gain, and required pump power. Typically, high pump powers in the 10–100-mW range are required, meaning, in turn, expensive 980-nm and 1480-nm lasers are necessary. Such pump lasers constitute a significant fraction of the cost of a planar amplifier. To avoid the use of a pump laser, a radically new approach is required. This is where sensitizers come in. A sensitizer coupled to an Er ion absorbs light at a cross section much larger than that of Er and

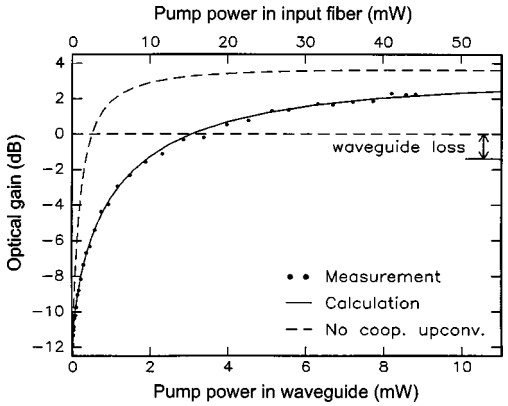

Fig. 3. Optical gain as a function of pump power measured on an Er-implanted miniature optical amplifier based on Al_2O_3; from van den Hoven *et al.*, Ref. 4.

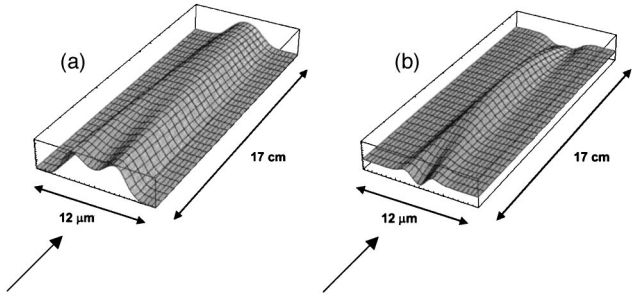

Fig. 4. Degree of inversion (a) and differential gain (b) along the length of the waveguide. Calculations are made for an Er-doped, Al_2O_3 ridge waveguide pumped at 100 mW at 1.48 μm with the pump direction indicated by the arrow. The dip in the front facet is caused by ESA. From Kik and Polman, Ref. 10.

then transfers its energy to Er. If the sensitizer has a broadband absorption spectrum it may be pumped by a white-light source or an LED, rather than a laser. In such a case, by choosing the proper pump wavelength, ESA may also be avoided.

C. Sensitizers for Erbium

In this paper we review sensitizers based on three classes of materials: (1) semiconductor nanocrystals, (2) metal ions, and (3) organic complexes. Before doing so, we first briefly discuss the well-known concept of Yb as a sensitizer for Er. While this concept has been well documented in the literature, and it is not the intent to review it fully here, we discuss it in Section 2 to demonstrate some of the general characteristics of a sensitizer, and show that it has a beneficial effect only under carefully chosen conditions of concentration, waveguide length, and pump power.

In Section 3, we describe Si nanocrystals as sensitizers for Er. They can be excited using a broadband light source, and they show strong coupling to Er. The energy transfer rates, efficiencies, and concentration limits are described, and measurements on a waveguide based on Si-nanocrystal-doped SiO_2 are presented. Then, in Section 4 we describe an entirely new concept, the use of Ag^+ ions in silica glass that have a very strong sensitizing effect on Er. Some details of the coupling between Ag^+ and Er are described. In Section 5, we describe rare-earth-doped, organic cage complexes that can be integrated with polymer waveguide technology. By taking advantage of the rich organic synthesis technology, a variety of sensitizers can be functionalized with the rare-earth-doped organic cage complexes. We demonstrate sensitizing effects of both the aromatic rings of the encapsulating ligand and aromatic moieties (such as lissamine) that are attached to rare-earth-doped complexes.

In Section 6 we describe a waveguide coupling geometry that is designed to optimize the coupling from a sensitizer to a rare earth in a planar integrated circuit. Section 7 summarizes and compares the sensitizing effects of the four materials described in this paper. Finally, in Section 8, we briefly outline how erbium can be used as a sensitizer itself, either to generate excitons in single-crystalline silicon or to excite thulium ions that then emit a broad infrared spectrum, and may permit optical amplifiers with very large bandwidth.

2. YTTERBIUM AS A SENSITIZER FOR ERBIUM

The Yb^{3+} ion's strong absorption at ≈980 nm has made it an obvious candidate for use as a sensitizer for Er.[12–16] Sensitization relies on the fact that the $^2F_{5/2}$ level of Yb^{3+} and the $^4I_{11/2}$ level of Er^{3+} are nearly resonant in energy. Yb^{3+} can be excited either by a pump laser in its relatively narrow 980-nm absorption band, or by a narrow-band light source that is absorbed in the broad 850–980-nm absorption band of Yb^{3+}.[17] As the Yb^{3+} absorption cross section at 980 nm is roughly ten times higher than that of Er^{3+},[18] pump radiation at 980 nm is efficiently absorbed and can then be transferred to Er^{3+} (see Fig. 5). This process is more power-efficient than direct excitation of Er^{3+} in many materials, i.e., per incoming photon, more Er^{3+} is excited per unit length. It should be noted that the reverse energy transfer process (backtransfer from Er^{3+} to Yb^{3+}) is also possible, and several studies have been devoted to minimizing this effect.[19,20] To determine the optimum Yb concentration for sensitizing erbium is not a trivial task: It is strongly linked to the waveguide cross section, the upconversion coefficient, and the ESA cross section. To illustrate this we have developed a rate-equation model, the details of which are described in Ref. 21. The processes taken into account are indicated in Fig. 5.

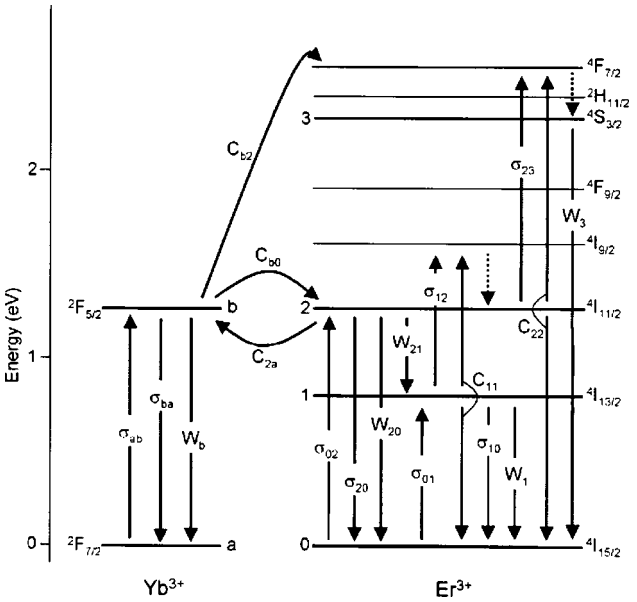

Fig. 5. Energy level diagram of Er^{3+} and Yb^{3+}. The arrows represent the processes included in the rate equation model used for the calculations. Included are absorption and stimulated emission processes σ_{ij}, spontaneous decays W_{ij}, and energy transfer processes C_{ij}. Dashed arrows represent spontaneous processes considered as instantaneous. From Strohhöfer and Polman, Ref. 21.

Calculations were performed for 2-μm wide, Al_2O_3 ridge waveguides embedded in SiO_2 (see inset in Fig. 6) that were homogeneously doped with Er and Yb. Most of the cross sections, decay rates, and energy transfer rates necessary as input to the model are known for Er-doped Al_2O_3.[18] Gain calculations were performed by assuming that only the fundamental mode at 980 nm is present in the waveguide. The effect of amplified stimulated emission was not taken into account. The development of the power in pump and signal mode was calculated over the length of the waveguide. Pump and signal were copropagating. First, we will discuss the signal output from Er^{3+}-doped ridge waveguides codoped with various concentrations of Yb^{3+}. The optimal Er^{3+} concentration ($3.35 \times 10^{20}\,cm^{-3}$) determined in previous work on pure Al_2O_3 waveguides (without Yb)[4,9] was used as the starting point in the calculations.

A. Gain for Fixed Waveguide Length

Figure 6 shows the small-signal gain as a function of launched pump power at 980 nm for a fixed waveguide length of 8 cm. Results for several Yb^{3+} concentrations

between 3.35×10^{20} and $26.8 \times 10^{20}\,\mathrm{cm}^{-3}$ are plotted, as well as for a waveguide doped only with Er^{3+}. At low pump powers the Er^{3+} is not inverted and most of the signal is absorbed (negative gain). In increasing the pump power we first notice an effect on the signal output of the waveguide containing no Yb^{3+}. As the Yb^{3+} concentration is increased, the curves in Fig. 6(a) show a smaller initial increase with pump power. This behavior is a result of the higher absorption cross section of Yb^{3+} with respect to Er^{3+}, which limits the propagation of the pump through the waveguide and thereby the length over which the Er^{3+} is inverted. The gain at 1530 nm is determined by the difference in populations of the Er^{3+} $^4I_{13/2}$ and $^4I_{15/2}$ energy manifolds averaged over the waveguide length.

Increasing the pump power further will eventually lead to a higher signal output for the Er^{3+}–Yb^{3+}-doped waveguide than for the Er^{3+}-doped waveguide. For example, for the waveguide with $3.35 \times 10^{20}\,\mathrm{Yb/cm}^3$, this crossover occurs at a launched pump power of ≈16 mW [see Fig. 6(a)]. The crossover will take place at higher pump powers as the Yb^{3+} concentration is increased. For very high pump powers, however, the signal output from all waveguides depends only on the Er^{3+} concentration and reaches the same value for all Yb^{3+} concentrations. This is the limit of full inversion of all Er^{3+} ions in the waveguide.

Figure 6(b) shows the corresponding data for a waveguide of 4-cm length. The details of this graph are the same as described for Fig. 6(a), although shifted to lower pump power. This is because the depletion of the pump is less for the shorter waveguide, thus, a greater fraction of the Er^{3+} is excited. However, the figure better illustrates the behavior at high pump powers, namely, the output signal's approaching its high-pump-power limit for all Yb^{3+} concentrations (the slight variations in gain at high pump powers reflect the differences in inversion of Er^{3+} in the tails of the signal mode).

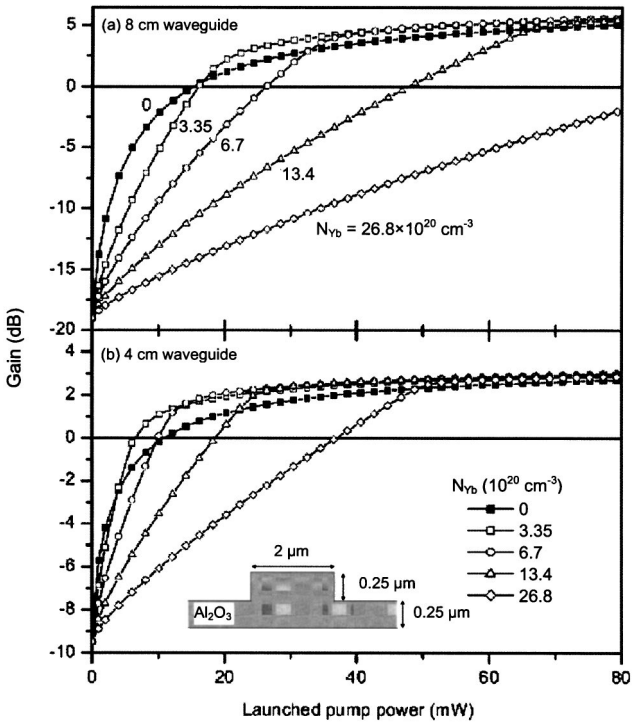

Fig. 6. Calculations of signal output from a waveguide of fixed length doped with $3.35 \times 10^{20}\,\mathrm{cm}^{-3}$ Er^{3+} as a function of launched pump power. Different curves represent different Yb^{3+} concentrations. Waveguide length, (a) 8 cm and (b) 4 cm. The inset shows a schematic of the waveguide cross section. From Strohhöfer and Polman, Ref. 21.

The saturation at high pump power naturally follows from the energy transfer mechanism between Yb^{3+} and Er^{3+}: The efficiency of the energy transfer from Yb^{3+} to Er^{3+} is limited by the transfer rate constant and the population in the Er^{3+} ground state (assuming for simplicity that the population of the Er^{3+} $^4I_{11/2}$ state is negligible, we can neglect Er → Yb energy backtransfer and energy transfer to higher-lying states). This means that by increasing the launched pump power we will eventually reach a regime in which the excitation of Er^{3+} by way of Yb^{3+} can be neglected compared with its direct excitation. This is due both to the depletion of the ground state population of Er^{3+} and to the limitation on the energy transfer resulting from the finite energy transfer rate constant, which is independent of pump power. If the amplifier is operated at such pump powers, Yb^{3+} codoping will have only a marginal effect (in our case, seen only in the tails of the mode) and so will be unnecessary.

On the low end of the power scale, there is, however, a rather clear correlation between gain threshold, length of the waveguide, and Yb^{3+} concentration. While for the 8-cm waveguide [Fig. 6(a)] the gain threshold for $N_{Yb} = 0$ and $N_{Yb} = 3.35 \times 10^{20}\,\mathrm{cm}^{-3}$ nearly coincides, we see that a waveguide of 4-cm length with concentrations of $N_{Yb} = 3.35 \times 10^{20}\,\mathrm{cm}^{-3}$ and $N_{Yb} = 6.7 \times 10^{20}\,\mathrm{cm}^{-3}$ has a lower gain threshold than a waveguide with no Yb^{3+}. For any waveguide length there is thus an Yb^{3+} concentration at which the threshold pump power has a minimum. More details are given in Ref. 21.

We thus conclude from Fig. 6 that the gain of an Er^{3+}-doped waveguide amplifier is improved significantly by Yb^{3+} codoping only if it is operated at a pump power around its threshold, under the condition that the Yb^{3+} concentration is not too high. A high Yb^{3+} concentration is countereffective as it causes a higher gain threshold and causes little improvement in gain over the case with no Yb^{3+}. The effect of the large absorption of Yb^{3+} on the gain has to be taken into account when designing Er–Yb-doped waveguide amplifiers.

B. Maximum Gain

In Fig. 7 we have plotted the results of calculations of the maximum gain as a function of launched pump power for several Yb^{3+} concentrations between 3.35×10^{20} and $26.8 \times 10^{20}\,\mathrm{cm}^{-3}$. Additionally, the calculated gain in a waveguide doped exclusively with Er^{3+} is depicted. Each point in the plot represents a waveguide whose length is optimized for maximum gain at a given pump power. This means that the waveguide length is chosen such that at its end the transparency condition, an average inversion of 50% over the cross section of the waveguide, is fulfilled. Consequently, the length of the waveguide differs for each of the points in the plot, both as a function of pump power for a given Yb^{3+} concentration and as a func-

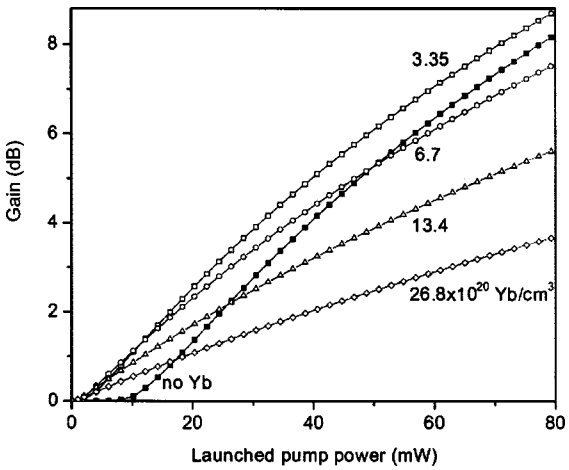

Fig. 7. Calculation of the maximum possible signal output from a waveguide doped with $3.35 \times 10^{20}\,\mathrm{cm}^{-3}\,\mathrm{Er}^{3+}$ as a function of launched pump power. Different symbols represent different concentrations of Yb^{3+}. The length of the waveguides has been adjusted for maximum gain for each Yb^{3+} concentration and each launched pump power. From Strohhöfer and Polman, Ref. 21.

tion of Yb^{3+} concentration itself. Over the pump power range represented, the length of the waveguide without Yb^{3+} varies between 0 and 18 cm and that of the waveguide doped with $26.8 \times 10^{20}\,Yb^{3+}/cm^3$ between 0 and 5.5 cm.

There are several noteworthy points about this plot. First, the threshold injected pump power for gain decreases with increasing Yb^{3+} concentration. This is a consequence of the higher excitation probability of Er^{3+} by way of Yb^{3+} at low pump powers, which is the result of the high absorption cross section of Yb^{3+} and efficient energy transfer toward Er^{3+}. Second, the slope of the curves, once the gain threshold is reached, decreases with increasing Yb^{3+} concentration. This is a signature of the higher conversion efficiency of absorbed pump photons for waveguides with smaller Yb^{3+} concentration. The lower the concentration of Yb^{3+}, the smaller the losses of pump energy caused by spontaneous decay of the Yb^{3+} ions. This feature becomes especially important for high inversion of the Er^{3+}, since in this case the probability is small that an excited Yb^{3+} ion can transfer its energy to an Er^{3+} ion in its ground state. This also implies that with increasing launched pump power, waveguides with higher Yb^{3+} concentration will eventually have less gain than waveguides with lower Yb^{3+} concentration. As a consequence, the maximum gain curves of waveguides with different Yb^{3+} concentrations will cross at a certain pump power. Several of these crossings can be seen in Fig. 7. Incidentally, the launched pump power at which these crossings occur should be independent of the inclusion of amplified spontaneous emission in the calculations, since amplified spontaneous emission depends—to first order—on the total inversion of the waveguide. For equal gain, this total inversion has to be equal for the two waveguides involved.

It is clear from Fig. 7 that for any given launched pump power, a properly chosen nonzero Yb^{3+} concentration will increase the maximum gain achievable in the waveguide over that with no Yb^{3+}. Although the curve given for a Yb^{3+} concentration of $3.35 \times 10^{20}\,\mathrm{cm}^{-3}$ (open squares) will eventually run below the curve for zero Yb^{3+} concentration (solid squares) for launched pump powers of more than 200 mW, decreasing the Yb^{3+} concentration further will shift the crossing toward even higher pump powers.

Finally, we address the relation between Yb^{3+} concentration and launched pump power necessary to achieve a fixed gain (again for optimized length). This corresponds to a horizontal cut through Fig. 7 and has been plotted in Fig. 8 for clarity. The solid symbols give the pump power that has to be launched into the waveguide to reach a certain gain as a function of Yb^{3+} concentration in the waveguide. It can be discerned that the launched pump power is minimal for a finite Yb^{3+} concentration. This minimum moves to lower values of the Yb^{3+} concentration as the gain augments. This behavior follows directly from the argument made above regarding the concentration dependence of the maximum gain. It is once again a consequence of the tradeoff between excitation efficiency of the Er^{3+} by way of Yb^{3+} and the increased absorption in the waveguide caused by Yb^{3+}. If too high an Yb^{3+} concentration is chosen, the pump power needed to achieve a certain gain level rapidly increases.

Included in Fig. 8 are two curves that show the waveguide lengths at which gains of 1.8 and 3 dB are achieved as a function of Yb^{3+} concentration (open symbols). The waveguide length is a decreasing function of Yb^{3+} concentration, which reflects the increased absorption in the waveguide due to Yb^{3+}. Reducing the length of a waveguide amplifier by Yb^{3+} codoping may hold interest from a device design point of view, but it is clear that the penalty paid in pump power for a small reduction of waveguide length is large beyond the Yb^{3+} concentration at which the required pump power has its minimum (see Fig. 8). This is because the shorter waveguide length has to be offset by gain in the tails of the mode and therefore an oversupply of power in the central part of the waveguide. In materials in which ESA of the pump radiation plays a role, this might actually have deleterious effects.

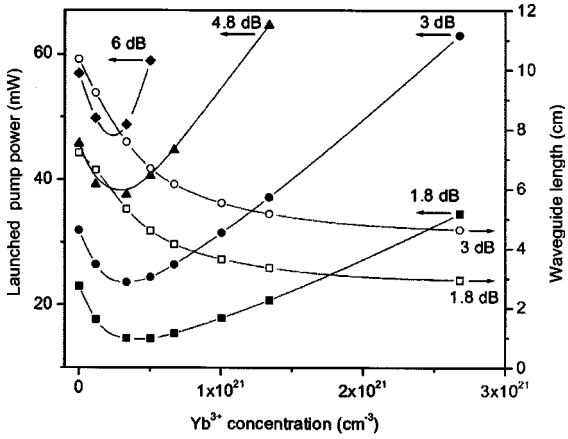

Fig. 8. Calculation of the pump power that has to be launched into the waveguide to reach a gain of 1.8, 3, 4.8, and 6 dB in a waveguide whose length has been optimized, as a function of Yb^{3+} concentration. Also plotted is the dependence of the waveguide length (optimized for maximum gain) on Yb^{3+} concentration for gains of 1.8 and 3 dB. The drawn curves are guides to the eye. From Strohhöfer and Polman, Ref. 21.

This section on Yb as a sensitizer gave a brief overview of the advantages and limitations of the use of a sensitizer for Er. Similar studies are required for the three sensitizer concepts that follow in Sections 3, 4 and 5, in which we take into account their absorption spectra and cross sections.

3. SILICON NANOCRYSTALS AS SENSITIZER FOR ERBIUM

Bulk semiconductors are the natural sensitizers for rare-earth ions. When embedded in a semiconductor, the rare earths act as point defects that generate defect levels in the bandgap. Optically or electrically generated carriers in the semiconductor can then become trapped at these defects to form a bound exciton. As the exciton has strong spatial overlap with the rare earth, it can recombine by transferring its energy to the rare earth (impurity Auger process). Er-doped bulk Si has been studied extensively.[22] One disadvantage of the bulk-semiconductor–Er system is that, because of the strong exciton-Er coupling, not only carrier-mediated excitation, but the reverse process, i.e., quenching of the Er by the generation of an exciton, can take place. This backtransfer is the major reason that in Si the Er luminescence is nearly fully quenched at room temperature.[23–25] This problem can be solved in two ways: by increasing the bandgap of the semiconductor so that the energy barrier for backtransfer is increased, or by decreasing the coupling between the exciton and the Er.[26,27]

We first briefly discuss the bandgap engineering option and then report on how the coupling can be reduced. The bandgap of Si can be enhanced by codoping with oxygen. We have studied a highly O- and H-doped Si material (SIPOS) that we doped with Er by ion implantation.[28] Photoluminescence excitation spectroscopy showed the Er was excited indirectly, i.e., through photocarriers in the amorphous semiconductor (bandgap ~2 eV). By taking advantage of the semiconducting nature, the Er could also be excited electrically, by impact excitation.[29] This first Er-doped, Si LED was reported several years ago.[30] Experiments were also performed on this same semiconductor upon its crystallization. In this case a highly connected nanosilicon network formed, embedded in SiO_2 and doped with Er. In this material a clear sensitizing effect was observed as well.[31] Photocarriers excited in the Si nanostructures lead to the excitation of Er ions in the oxide matrix. Because the carrier lifetime in the highly defective Si nanostructures was small, the overall Er sensitization efficiency was well below 100%.

Recently, Fujii *et al.*[32] reported that the presence of Si nanocrystals in Er-doped SiO_2 considerably enhances the effective Er absorption cross section. This material is quite different in structure from crystalline SIPOS; the Si nanocrystals are randomly dispersed in the matrix, are single-crystalline, spherical in size, and spaced at distances in the 2–5-nm range, depending on the concentration. Depending on the preparation condition, they may have very low nonradiative internal recombination rates, thus enabling high sensitization efficiency. Following this observation, a number of papers appeared that showed similar results for similar materials prepared using different techniques.[33–36] All observations strongly suggest that energy is transferred from Si nanocrystals to Er ions in the SiO_2 matrix. The excitation and energy transfer model is given in Fig. 9(a), which shows a schematic band diagram of SiO_2 containing a Si nanocrystal and an Er^{3+} ion. First, a photon is absorbed by the nanocrystal, which causes generation of an exciton bound in the nanocrystal. The exciton can recombine radiatively, emitting a photon with an energy that depends on the nanocrystal size. Alternatively, if an Er ion is present close to the nanocrystal, the exciton can recombine nonradiatively by bringing Er into one of its excited states. To study this process in detail we fabricated Si nanocrystals in thermally grown SiO_2 at a density of 10^{19} nanocrystals/cm^3, and doped this material with Er by ion implantation. Details of the fabrication process are described in Refs. 37–39.

A. Nanocrystal–Erbium Energy Transfer Rate and Efficiency

Figure 10 shows photoluminescence (PL) spectra taken at 20, 60, 180, and 300 K at a pump power of 10 mW for a sample doped to an Er peak concentration of 1.8 at.%. At all temperatures a broad luminescence band is observed extending from 0.6 μm to 1.1 μm that is attributed to the radiative recombination of excitons localized at Si nanocrystals. The exciton luminescence appears at energies above the bandgap energy of bulk Si as a result of quantum confinement.[40] The large spectral width of the nanocrystal luminescence is the result of the rather broad nanocrystal size distribution (diameter 2–5 nm) in addition to homogeneous broadening.[41]

Superimposed on the nanocrystal PL spectrum, a relatively sharp peak is observed at 982 nm corresponding to the $^4I_{11/2} \rightarrow {}^4I_{15/2}$ transition of Er^{3+}. Another clear emission line is observed at a wavelength of 1536 nm corresponding to the $^4I_{13/2} \rightarrow {}^4I_{15/2}$ transition of Er^{3+}. Figure 11 shows a PL excitation spectrum in which both the nanocrystal emission at 750 nm and the Er emission at 1.53 μm are plotted versus pump wavelength.[42] The smooth dependence of the Er signal on wavelength indicates that the Er is not excited directly by optical absorption, but indirectly by energy transfer involving Si nanocrystals.[32,33,36] The excitation spectra show that at a fixed pump power, the nanocrystal luminescence inten-

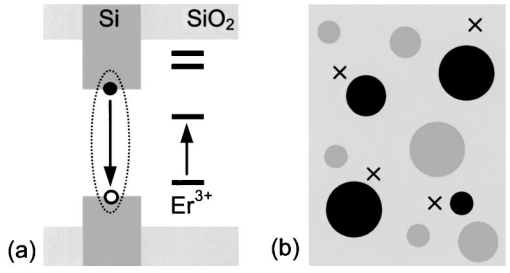

Fig. 9. (a) Schematic Er excitation model showing the electronic band structure of Si-nanocrystal-doped SiO_2 and the Er $4f$ energy levels. An optically generated exciton (dotted ellipse) confined in the nanocrystal can recombine and excite Er^{3+}. (b) Schematic representation of SiO_2 containing Er (crosses) and nanocrystals (circles). The nanocrystals that couple to Er (black circles) show no exciton luminescence. From Kik *et al.*, Ref. 37.

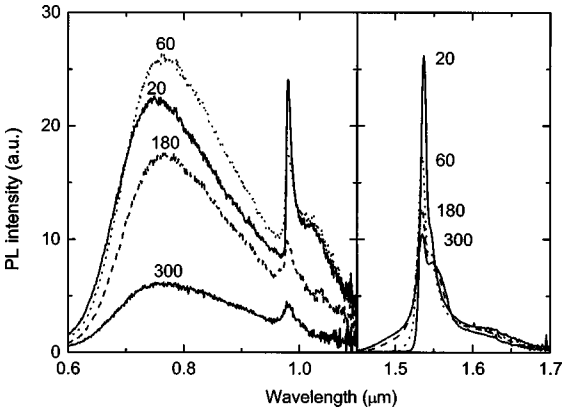

Fig. 10. Photoluminescence spectra at 20, 60, 180 and 300 K showing a broad nanocrystal spectrum in the range 600–1100 nm and two clear Er^{3+} luminescence lines at 982 nm and 1536 nm. The Er concentration was 1.8 at.%. $\lambda_{pump} = 458$ nm, 1 mW. From Kik *et al.*, Ref. 37.

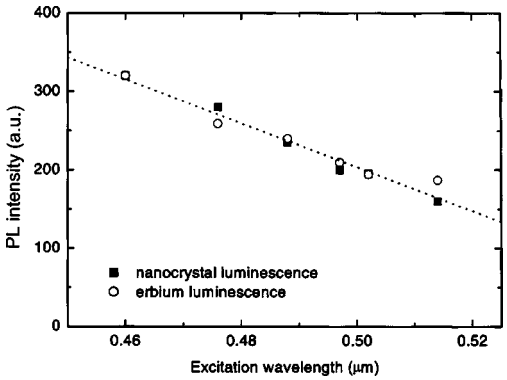

Fig. 11. Excitation spectrum of the nanocrystal luminescence at 750 nm and the Er^{3+} luminescence at 1526 nm. The dotted curve is a guide to the eye. From Kik, Ref. 42.

sity and the Er luminescence intensity increase by a factor of two when the excitation wavelength is decreased from 514 nm to 459 nm. This is due to the increasing nanocrystal optical absorption cross section for increasing photon energy.[43]

In Fig. 10 it can be seen that increasing the temperature from 20 to 300 K first causes the nanocrystal luminescence to increase by 16% and then to decrease by 75% on going from 60 to 300 K. This kind of temperature dependence is commonly observed for Si nanocrystals, and can be described fully by a model that takes into account the temperature-dependent population of the exciton singlet and triplet states (with high and low radiative decay rates, respectively) in competition with nonradiative processes.[44] The Er luminescence peak at 1536 nm exhibits an entirely different temperature dependence. The temperature increase only induces spectral broadening as a result of the thermal redistribution over the Stark levels, while the integrated intensity remains constant within 10%.

Figure 12 shows decay curves of the nanocrystal luminescence at 750 nm (a) and the Er luminescence at 1536 nm (b), measured at 15 K and 300 K at a pump power of 1 mW for the same sample as in Fig. 11 (1.8 at.% Er). It is found that the nanocrystal decay rate increases from 1.5 $\times$ $10^3\,s^{-1}$ to $4.8 \times 10^4\,s^{-1}$ upon increasing the temperature from 15 to 300 K, which is consistent with the exciton singlet–triplet model.[44] The Er decay time at 1536 nm is found to be 2.1 ms at all temperatures between 20 and 300 K, which implies that the Er transition at 1.5 μm is not quenched at room temperature.

A consistent description of the observed temperature dependences can be obtained if we assume efficient coupling between a Si nanocrystal and Er. If the energy transfer from a nanocrystal to Er is fast, we expect to see no luminescence from a nanocrystal that is coupled to Er, since any generated exciton will immediately recombine nonradiatively by exciting Er. Such fast transfer might occur because at the high nanocrystal density ($\approx 10^{19}\,cm^{-3}$) the maximum distance between an Er ion and the nearest nanocrystal is $\approx$1 nm. This implies that the exciton wave function has significant overlap with the Er $4f$ electrons. The Er luminescence intensity will then be determined by the product of the nanocrystal absorption cross section, which is approximately temperature independent, and the Er luminescence efficiency, which is also temperature independent [Fig. 12(b)].

The fact that the Er luminescence intensity is constant up to room temperature implies that the energy transfer to Er occurs well within the nanocrystal decay time at 300 K, which is 21 μs. Consequently the transfer rate constant must be larger than $\approx 10^6\,s^{-1}$ at room temperature. In this case all observed nanocrystal luminescence originates from nanocrystals that do not couple to Er, while nanocrystals that do couple to Er show no luminescence. This model is shown schematically in Fig. 9(b). Note that in this model the coupling is strong enough to quench the nanocrystal luminescence. At the same time, it must be weak enough that energy backtransfer from excited Er to the nanocrystal does not occur. The spatial separation between the nanocrystal and Er, and hence moderate overlap between exciton and Er, then leads to this intermediate and desired coupling. Indeed, the coupling constant measured for nanocrystal–Er coupling is several orders of magnitude smaller than that for Er in bulk Si, in which strong energy backtransfer is observed.[25]

To determine the Er excitation efficiency, we measured the time dependence of the nanocrystal and Er lumines-

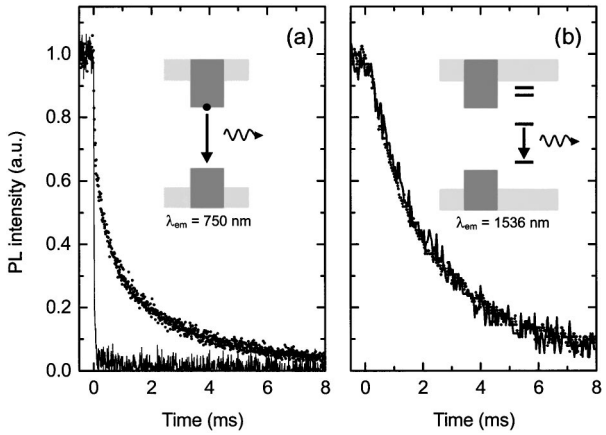

Fig. 12. Luminescence decay measurements taken at 15 K (dots) and at 300 K (drawn lines) of (a) nanocrystal luminescence at 750 nm, and (b) Er^{3+} luminescence at 1536 nm. $\lambda_{pump} = 458$ nm, 1 mW. From Kik *et al.*, Ref. 37.

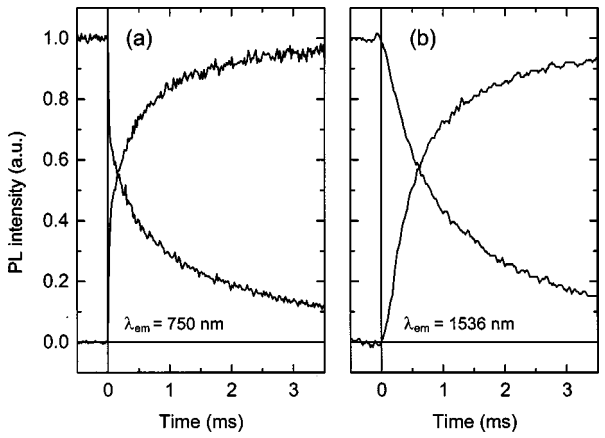

Fig. 13. PL intensity measured as the 5 mW pump beam is switched on and off, measured at 15 K for (a) nanocrystal luminescence at 750 nm, and (b) Er luminescence at 1536 nm. $\lambda_{pump} = 458$ nm. From Kik and Polman, Ref. 38.

cence intensity as the pump beam is switched on and off, again for the sample with 1.8 at.% Er (Fig. 13). The curves measured on switching on the pump show an initial rise followed by saturation, which corresponds to an initial increase in the population of excited Er followed by buildup of a steady-state population. The curves measured on switching off the pump show the gradual decrease in excited Er population due to spontaneous decay. From the data in Fig. 13, taken at a pump power of 5 mW at 15 K, we derive the luminescence $1/e$ rise time (τ_r) and decay time (τ_d), from which the excitation rate $R = (1/\tau_r - 1/\tau_d)$ can be deduced, assuming that the Er and the nanocrystals effectively behave as two-level systems. At a pump intensity of 5 mW/mm^2 we find for the nanocrystal excitation rate $R_{nc} = 940\,s^{-1}$ and for the Er excitation rate $R_{Er} = 570\,s^{-1}$. Note that this Er excitation rate may contain a contribution of excitation into the higher-lying Er energy levels, followed by nonradiative relaxation to the first excited state. Comparing the nanocrystal and Er excitation rates, we conclude that at least 60% of the generated excitons recombine by transferring energy to Er.[45] This high conversion efficiency is in agreement with the intermediate coupling model.

B. Erbium Concentration Limit

The high excitation efficiency also raises a new question. At the peak concentration of 1.8 at.% Er, the Er-to-nanocrystal ratio is ≈100:1, which implies that in principle many Er ions compete for the same exciton. Nevertheless, the observed Er excitation rate (per ion) is close to that of a single nanocrystal. This leads to the conclusion that a single nanocrystal can effectively excite only ≈1–2 Er ions. This observation, together with the estimated nanocrystal concentration of $10^{19}\,cm^{-3}$, implies that the maximum excitable Er concentration is ≈$(1–2) \times 10^{19}\,cm^{-3}$ (≈0.02–0.04 at.%).

To study this effect in more detail, PL spectra were taken of different samples with Er concentrations in the range 0.015–1.8 at.%. All data were taken at 15 K and are plotted in Fig. 14. A spectrum for a sample containing nanocrystals only is also shown. It shows the broad luminescence due to the radiative recombination of quantum-confined excitons in nanocrystals with a broad size distribution. The incorporation of 0.015 at.% Er reduces the nanocrystal luminescence by more than a factor of two, and a luminescence peak due to Er appears at a wavelength of 1536 nm. Increasing the Er concentration leads to a further reduction of the nanocrystal luminescence intensity, accompanied by an increase of the Er luminescence intensity. This behavior is consistent with the intermediate coupling model, in which a nanocrystal becomes "dark" once it couples to a nearby Er ion. Increasing the Er concentration therefore increases the fraction of dark nanocrystals. A saturation in the Er PL intensity is observed as the Er concentration exceeds 0.17 at.%. As can be seen in Fig. 15, even for the highest Er concentrations, some nanocrystal luminescence is observed. This is attributed to the fact that the Er implantation depth profile in this particular sample is slightly deeper than the Si nanocrystal depth profile,[38] so that some nanocrystals in the near-surface region do not couple to Er.

To determine the concentration-dependent Er excitation rate, we performed rise time and decay time mea-

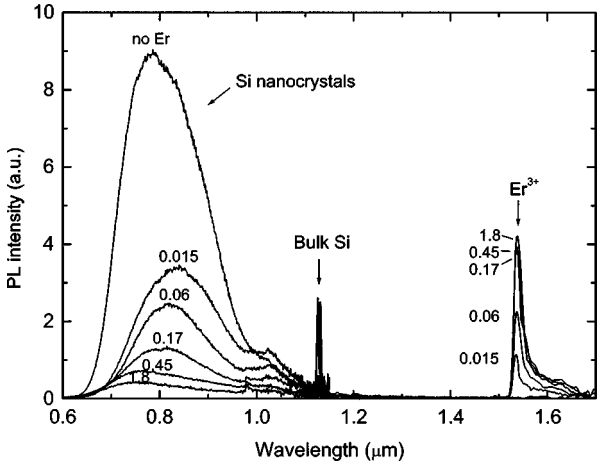

Fig. 14. Photoluminescence spectra of Si-nanocrystal-doped SiO_2 containing different Er^{3+} concentrations in the range 0–1.8 at.%, measured at 15 K with pump power of 1 mW at 458 nm. From Kik and Polman, Ref. 38.

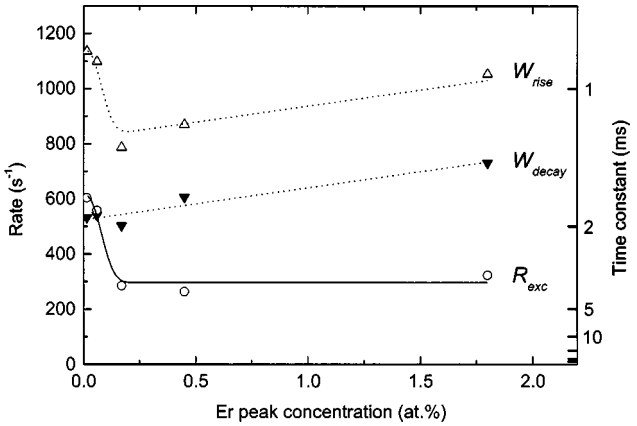

Fig. 15. Rise times (open triangles) and decay times (filled triangles) of the 1536-nm Er luminescence measured at 15 K at a pump power of 1 mW at 458 nm, and the Er^{3+} excitation rate derived from these data (open circles). The drawn curves serve as guides to the eye. From Kik and Polman, Ref. 38.

surements of the Er luminescence at 1536 nm. At the applied pump power of 1 mW all samples show approximately exponential time dependences. Figure 15 shows the measured rates $W_{\text{rise}} = 1/\tau_{\text{rise}}$ and $W_{\text{decay}} = 1/\tau_{\text{decay}}$ obtained by exponential fitting of the data. The Er decay rate increases from 500 s^{-1} to 700 s^{-1} as the Er peak concentration is increased from 0.015 at.% to 1.8 at.%. This increase is attributed to a concentration-quenching effect that is known to occur when rare-earth ions are spaced closely enough to allow for energy exchange between neighboring ions. As a result, excitation energy can migrate to neighboring ions, which may in turn be coupled nonradiatively to quenching sites, e.g., defects or OH groups present in the matrix.[1] In a simple concentration-quenching model, the Er decay rate increases linearly with Er concentration, which is indeed observed in Fig. 15. By measuring the slope of the decay rate data in Fig. 15 we can estimate[46] that the concentration of quenching sites in the Er-implanted, Si-nanocrystal-doped SiO_2 film is as low as 10^{18} cm^{-3}.

Data for the Er excitation rate $R_{\text{exc}} = (1/\tau_r - 1/\tau_d)$ are also shown in Fig. 15. At an Er concentration of 0.015 at.%, the Er excitation rate is 600 s^{-1}. Increasing the Er concentration to 0.17 at.% reduces the excitation rate by a factor of 2. A further increase of the Er concentration has no effect on the excitation rate, even though at these concentrations several Er ions might couple to the same nanocrystal, which would reduce the excitation rate per Er ion. That such a reduction is not observed shows there is an upper limit to the number of Er ions that can be excited by a single nanocrystal. From the data in Fig. 16 it is clear that this limit is reached at an Er concentration <0.17 at.%. This is consistent with the limit of 0.02–0.04 at.% found above.

The data in Fig. 14 show a sublinear increase of the Er intensity with concentration. This can be ascribed to the fact that as the Er concentration is increased, the exciton concentration available for Er excitation is reduced. At sufficiently high pump power, however, the Er luminescence intensity is no longer limited by the exciton concentration but rather by the total amount of excitable Er. Therefore, we can compare the total amount of excitable Er in samples with different Er concentrations by comparing Er luminescence intensities at high pump power.

Figure 16 shows the pump power dependence of the Er (1536 nm) and nanocrystal (750 nm) luminescence intensity for samples containing 0.015 at.% Er and 1.8 at.% Er. For both samples the nanocrystal luminescence intensity was scaled to coincide with the low-power Er luminescence intensity. Below 20 μW the Er luminescence and the nanocrystal luminescence depend linearly on pump power. At these low pump powers the Er luminescence intensities from the two samples differ by a factor of ≈ 2. Increasing the pump power leads to a sublinear increase of the Er luminescence in both samples, suggesting that a significant fraction of the excitable Er is brought into the first excited state. At a pump power of 50 mW the nanocrystal luminescence continues to increase, while the Er luminescence intensity levels off. Hence, in this pump power regime the exciton generation rate is no longer the limiting factor for the Er luminescence intensity. Nevertheless, the Er luminescence intensities for the two

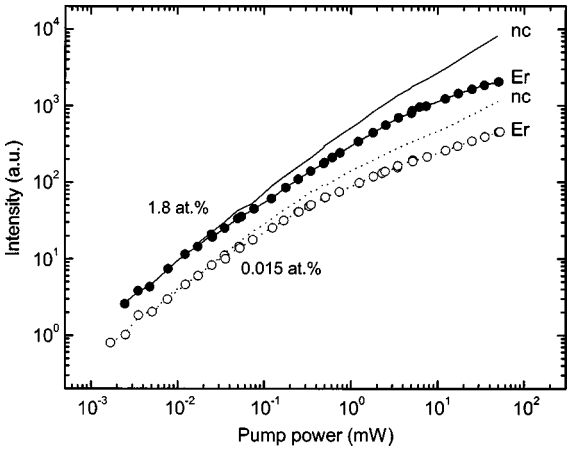

Fig. 16. Photoluminescence intensity of the nanocrystal luminescence at 750 nm and the Er^{3+} luminescence at 1536 nm as a function of pump power for samples containing 0.015 at.% and 1.8 at.% Er measured at 15 K with 458-nm pump beam in a ≈ 1 mm^2 spot. From Kik and Polman, Ref. 38.

samples at 50 mW pump power differ by only a factor of 5, even though the total amount of Er in the samples differs by more than a factor of 100. This shows that the concentration of excitable Er in the high concentration (1.8 at.%) sample is at most 5 times higher than in the low concentration (0.015 at.%) sample, suggesting that the concentration of excitable Er is <0.1 at.%. This is consistent with the concentration limit of <0.17 at.% Er found above.

C. Models Describing the Erbium Concentration Limit

The existence of an upper limit to the amount of excitable Er could indicate that there is a limit to the amount of optically active Er that can be incorporated in this material. This may, for example, be caused by Er clustering or $ErSi_2$ formation at the Si–SiO_2 interface, which would prevent the Er from being in the 3+ valence state. However, measurements on Er- and Si-nanocrystal-doped waveguides show a strong Er^{3+}-related absorption,[39] suggesting that a large fraction of the Er be in the optically active state.

Alternatively, the observed concentration limit could be an intrinsic property of the excitation process. The amount of excitable Er is low when the effective Er excitation efficiency is influenced by the presence of *excited* Er. Two models that would explain such behavior are:

1. Auger de-excitation, in which the already excited Er ion transfers its energy to an exciton generated in the nearby nanocrystal. A similar process has been shown to occur in Er-doped bulk Si.[47] After such Auger de-excitation the exciton can relax and subsequently excite an Er ion, effectively bringing the system back to the situation before the exciton was formed; or

2. Pair-induced quenching, in which two excited Er ions can interact, yielding one Er ion in the $^4I_{9/2}$ state that rapidly decays to the first excited state, and one Er ion in the ground state. This cooperative upconversion effect usually causes a shortening of the Er decay rate at high pump powers, which was not observed. However, if

the Er–Er coupling is sufficiently strong, no effect on the lifetime is seen. This special case is usually called pair-induced quenching.

From the measured Er excitation rate of $\approx 300\ s^{-1}$ at 1 mW (Fig. 15) we can determine an effective absorption cross section σ_{eff} for the Er excitation process. We find that $\sigma_{eff} \approx 10^{-15}\,cm^2$ at 458 nm, which is a factor of 10^5–10^6 larger than what can be achieved by using direct optical pumping of the Er ions, and similar to the Si nanocrystal absorption cross section at a pump wavelength of 458 nm.[43] This high cross section makes this nanocrystal sensitization concept ideal for application in waveguide amplifiers. Because of the wide nanocrystal absorption spectrum the pump wavelength can now be chosen over a broad spectral range. In fact, a LED or broadband white light source may now be used as a pump.

D. Gain-Limiting Processes in Erbium-Doped Silicon-Nanocrystal Waveguides in SiO_2

A Si-nanocrystal-sensitized, Er-doped optical waveguide was fabricated as described in Ref. 39. Figure 17(a) shows the Er and Si concentration depth profiles. The Si concentration profile peaks at a depth of 240 nm at a peak concentration of 42 at.%, corresponding to an excess Si concentration of 13 at.%. Assuming an average nanocrystal diameter of 3 nm,[48] the nanocrystal concentration at the peak of the Si profile is estimated to be $1.3 \times 10^{19}\,cm^{-3}$. The Er concentration profile peaks at a depth of 240 nm at a peak concentration of $N_{Er} = 8.3 \times 10^{20}\,cm^{-3}$ (i.e., ≈50 Er ions per Si nanocrystal).

A series of 3.5-μm-wide ridge waveguides was formed in the implanted and annealed SiO_2 film by standard photolithography and Ar beam etching to a depth of 0.5 μm, i.e., well beyond the Si-doped region. The excess Si inside the ridges locally raises the index of refraction, providing the index contrast required for optical mode confinement. To reduce scattering losses, the waveguides were covered with a 1.25-μm thick SiO_2 cladding layer by means of microwave sputtering. The samples were subsequently cut to a length of 8 mm, and the waveguide input and output facets were mechanically polished. A sketch of the final structure is drawn in Fig. 17(b), where $y = 0$ corresponds to the position of the SiO_2 surface before the etching process. The light gray area represents the remaining SiO_2 after etching of the ridge, and the location of the implanted Er and Si is indicated by the dark gray line at $y = 0.24\,\mu m$. The smooth solid line at $y \approx 1\,\mu m$ corresponds to the sample surface after deposition of the SiO_2 cladding layer.

Figure 17(b) shows iso-intensity contours of the optical mode image at 1.49-μm light from an InGaAsP laser guided through the waveguide. The emission from the output facet was projected onto an infrared camera by a microscope objective. At this wavelength the waveguide supports only the fundamental mode. The mode is slightly elliptical, with a FWHM of 3.8 μm in the x direction and 3.1 μm in the y direction (uncorrected for imaging resolution). In this particular sample structure, with only a small section of the waveguide doped with Er, the Er-related absorption and gain will be small, as the effective overlap Γ of the optical mode with the Er profile is only 1%. This low value can easily be increased by changing the size of the nanocrystal-doped core by performing multiple Er and Si implants, or by depositing a layer of Er- and Si-doped SiO_2, e.g., by using sputter deposition[33] or chemical vapor deposition.[49]

Figure 18(a) shows normalized transmission spectra of Si nanocrystal waveguides containing no Er (dotted curve) and 1.3 at.% Er (solid curve), measured by using a broadband light source butt-coupled to the nanocrystal waveguide by a single-mode tapered fiber. In the Er-doped sample a clear dip is observed at ≈1.53 μm due to the $^4I_{15/2} \rightarrow {}^4I_{13/2}$ absorption transition of Er^{3+}. The Er-related absorption obtained by dividing the normalized curves in Fig. 18(a) is shown in Fig. 18(b) (solid curve). The peak absorption at 1.532 μm is found to be 2.7 dB/cm. From the calculated mode overlap with the Er-doped

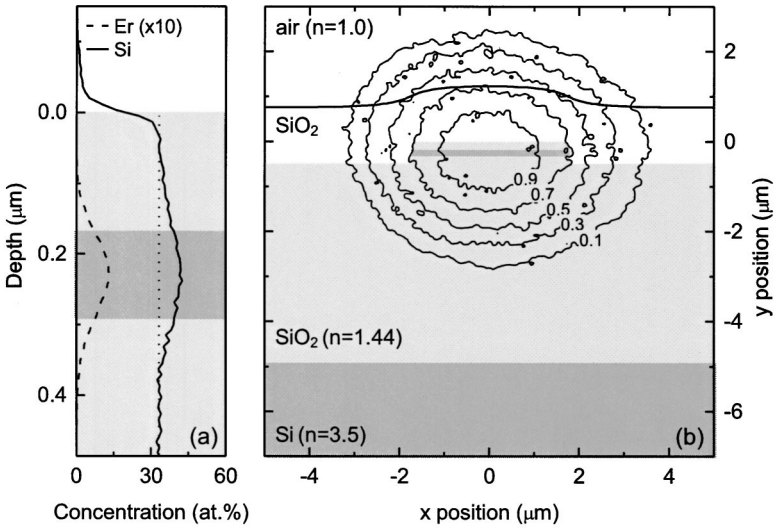

Fig. 17. (a) Er and Si concentration profiles in an ion-implanted planar waveguide sample as determined by Rutherford backscattering spectroscopy. (b) Optical mode image at a wavelength of 1.49 μm taken at the output facet of an Er^{3+}-doped Si-nanocrystal-based ridge waveguide. The contour lines indicate constant intensity. A sketch of the waveguide structure is included. From Kik and Polman, Ref. 39.

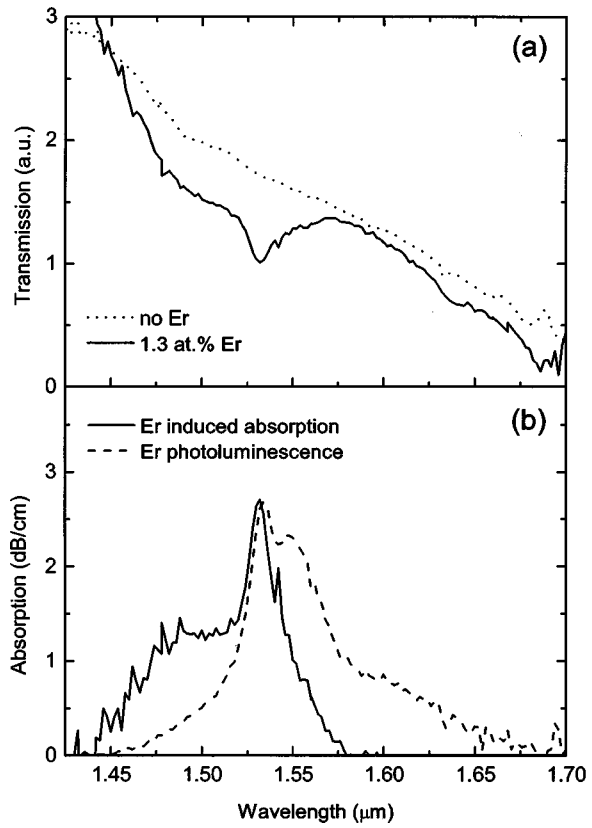

Fig. 18. (a) Normalized transmission spectra of Si-nanocrystal-based waveguides containing no Er (dotted curve) and 1.3 at.% Er (solid curve). (b) Er-related absorption spectrum (solid curve) derived from the data in (a) and Er photoluminescence spectrum (dashed curve) collected at the waveguide output facet (pump power 180 mW at 458 nm). From Kik and Polman, Ref. 39.

layer, the absorption cross section at 1535 nm was derived: $\sigma = 8 \times 10^{-20}\,\mathrm{cm}^2$. This value is more than a factor of 10 larger than values found in Er-doped Si ($2 \times 10^{-20}\,\mathrm{cm}^2$)[25] and SiO_2 ($\approx 4 \times 10^{-21}\,\mathrm{cm}^2$). Additional evidence for such an unusually high cross section has also been found later by Han *et al.*[50] and Pacifici *et al.*[51] The large cross section may be due to the strong asymmetry of the local dielectric environment of the excitable Er^{3+} ions (note that in a perfectly symmetrical geometry the $^4I_{13/2} \rightarrow {}^4I_{15/2}$ transition is parity forbidden). This may also explain the relatively short luminescence lifetimes typically observed in this type of material. The high absorption cross section would also translate into a high emission cross section,[52,53] which implies that high gain could be achieved in this material over a short length.

Optical pumping was achieved by projecting a 458-nm laser beam onto the top of the waveguide by a cylindrical lens. The elongated spot was aligned with the waveguide and evenly covered the full waveguide length. Figure 18(b) shows the spectrum of guided Er PL collected at the output facet. The spectral shape was found to be independent of the applied pump power in the range 25–180 mW. From PL rise and decay time measurements at 1.535 μm it follows that at the lowest applied pump power (25 mW) the Er excitation rate R_{Er} is at least 570 s^{-1}, which would be sufficient to keep 70% of the excitable Er in the first excited state.

Next, optical gain measurements were performed by measuring transmission spectra as a function of pump power. It was found in this sample that even at a pump power as high as 250 mW, no change in the Er-related absorption could be detected within the measurement accuracy. This puts an upper limit on the amount of Er in the waveguide that is excited through Si nanocrystals. On the basis of experimentally obtained values for σ_{Er} and Γ and the known noise in our transmission spectra of 1%, we conclude that the concentration of inverted Er ions in the Si-nanocrystal-doped region must have been less than $3 \times 10^{19}\,\mathrm{cm}^{-3}$. Given the implanted peak Er concentration of $8.2 \times 10^{20}\,\mathrm{cm}^{-3}$, this implies there is a large unbleachable fraction of Er in the waveguide, so no gain is achieved. That the maximum excitable Er concentration is close to the estimated nanocrystal peak concentration of $1.3 \times 10^{19}\,\mathrm{cm}^{-3}$ in our samples provides further evidence for the hypothesis[37,38] that the amount of excitable Er in Si-nanocrystal-doped SiO_2 is limited to $\approx$1 Er ion per nanocrystal.

Finally, we note that recently Han *et al.* reported that data on an optimized Er- and Si-nanocrystal-doped waveguide showed a strong signal enhancement at 1.53 μm under optical pumping. Provided the waveguide losses are low, this would point to the achievement of net optical gain.[54]

4. SILVER AS A SENSITIZER FOR ERBIUM

In the search for sensitizers for Er, we have also studied PL-enhancement effects that Ag might have on Er^{3+} in oxide glass.[55] Ag can be introduced easily to concentrations of several atomic percent into glasses by an ion exchange process,[56] interchanging network modifiers of the glass such as Na^+ or K^+ with Ag^+ ions. This is a standard process for fabricating waveguides for integrated optics. Several absorption and emission bands in the visible and near ultraviolet related to Ag have been observed in glasses,[57,58] opening the possibility of energy transfer toward Er^{3+}. Doping glasses with Ag, however, gains an additional dimension in that nanometer-sized crystals can be precipitated.

In the following we will report investigations of borosilicate glass doped with Er by ion implantation and with Ag by ion exchange. By adjusting the doping procedure we are able to fabricate samples with a high concentration of dissolved Ag and little or no Ag nanocrystals, and samples in which a considerable amount (but not all) of the Ag aggregates into crystallites.

The borosilicate glass substrates we used for these experiments were 1-mm thick Schott BK7 wafers. Ag was introduced into the samples by a $Na^+ \leftrightarrow Ag^+$ ion exchange in a salt melt containing 5 mol.% $AgNO_3$ and 95 mol.% $NaNO_3$. The samples were left in the melt for 7 min at 310°C. Er was implanted at an energy of 925 keV to a fluence of $3.1 \times 10^{15}\,\mathrm{cm}^{-2}$ in the glass substrate at liquid nitrogen temperature. Two samples were prepared combining these two doping techniques. One was first implanted with Er and subsequently ion-exchanged, while the other underwent the ion exchange first, and the resulting Ag^+-doped glass was then implanted with Er. The bombardment of Ag^+-doped glass with heavy ions, as

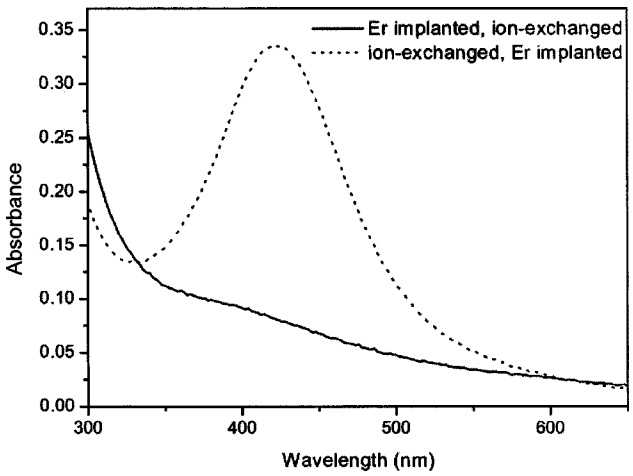

Fig. 19. Absorbance of silica glass samples doped with Er and Ag. The band at ≈420 nm is caused by the plasmon resonance of Ag nanocrystals formed during Er implantation into Ag-containing glass. The data were measured relative to an untreated reference glass slide.

in the latter case, has been shown to lead to the formation of Ag nanocrystals.[59] For reference purposes, another glass sample was implanted with Er under the same conditions, but did not undergo ion exchange. All samples were annealed in vacuum for 30 min at 350 °C.

From Rutherford backscattering spectrometry we obtain a silver concentration of 2.2 at.% in the sample first ion-exchanged, then Er implanted, and ≈3 at.% for the sample implanted with Er before the ion exchange. These values are approximately constant up to a depth of ≈600 nm. For comparison, the Er range for our implantations amounts to 250 nm. We attribute the difference in Ag^+ concentration between the two samples to variations in the diffusivity of Ag^+ ions due to damage by the ion irradiation in the glass. While Ag is present predominantly as Ag^+ ions in the sample implanted with Er before ion exchange, irradiation with heavy ions after ion exchange leads to the agglomeration of a considerable amount of the Ag ions into metallic nanocrystals.[59]

Normal-incidence transmission spectra were measured on a dual-beam photospectrometer in the wavelength range between 300 and 2000 nm. An untreated glass slide was placed in the reference beam to measure changes in the transmission spectrum caused only by the various treatments of the samples. Figure 19 compares the absorbance induced by the preparation of the two samples doped with Ag and Er. The distinctive band peaking at 420 nm observed for the sample ion-implanted after ion exchange is caused by the surface plasmon resonance in the Ag nanocrystals. The fraction of Ag agglomerated in nanocrystals estimated from the strength of the absorption is ≈30%. The sample that was ion-exchanged after Er implantation shows an increased absorbance, rising toward shorter wavelengths, whose origin might be related to the ion exchange. A similarly shaped, yet slightly lower, structure underlies the surface plasmon band.

In Fig. 20 we have plotted the normalized emission spectra of the three samples (including the reference sample containing no Ag^+) between 1400 and 1700 nm. The spectra are identical for the three samples. While the luminescence of the sample without Ag has been excited with 488-nm radiation into the $^4F_{7/2}$ state of Er^{3+}, the samples containing Ag show strong PL even when excited with 476-nm light, a wavelength at which Er^{3+} does not absorb. This is illustrated by the excitation spectrum for the sample doped only with Er in Fig. 21(a), measured by using the lines from the Ar^+ laser. Only when excited at 515, 488, and 360 nm is significant emission from Er^{3+} at ≈1540 nm observed. In contrast, Er^{3+} can be excited over a wide spectral range in both samples containing Ag, extending from the near ultraviolet to the red, as is evident from Fig. 21(b). Note the difference in the intensity scale between Figs. 21(a) and (b), calibrated by PL inten-

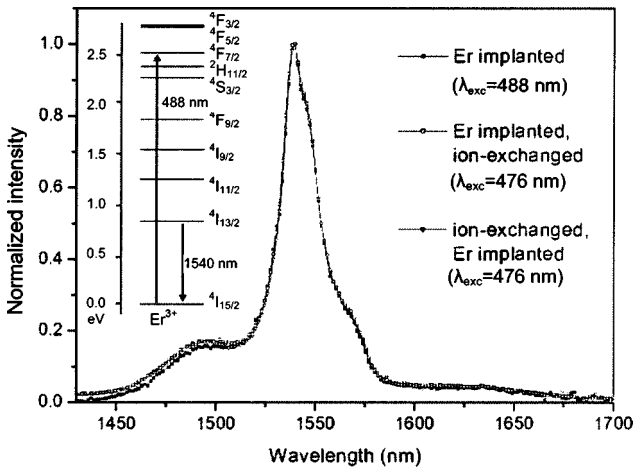

Fig. 20. PL spectra of Er-doped borosilicate glass doped with Ag by an ion exchange process (open symbols). Note that the Er^{3+} was excited at a wavelength which cannot be absorbed directly by Er^{3+}. The emission spectra are identical to the one obtained for Er^{3+} in glass without Ag when excited to its $^4F_{7/2}$ state (solid squares). The inset shows the energy level spectrum of Er^{3+}. From Strohhöfer and Polman, Ref. 55.

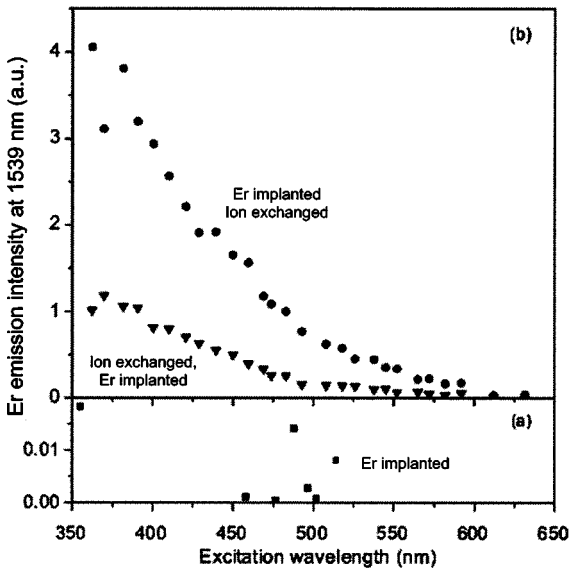

Fig. 21. PL intensity at 1539 nm as a function of excitation wavelength for three different samples; (a) borosilicate glass doped with Er only, (b) Er- and Ag-doped borosilicate glass. From Strohhöfer and Polman, Ref. 55.

sity measurements excited with the 488-nm line of the Ar^+ laser. The emission intensity at 1540 nm is enhanced by a factor of 20 and 70 for the samples with and without Ag nanocrystals, respectively, when they are excited with 488-nm radiation. Another fourfold increase of the Er^{3+} PL is achieved by reducing the pump wavelength from 488 to 360 nm. The PL lifetime measured at 1538 nm is 2.5 ms for the sample doped only with Er and 1.0 ms for the samples doped with Er and Ag.

Interestingly, in Fig. 21(b) the shape of the excitation spectrum for the two Ag-doped samples is identical. The sensitizing effect is larger for the sample that was first implanted and then ion-exchanged. This is the sample that has no Ag nanocrystals (or only a small number) and the larger Ag concentration dispersed as Ag^+ ions. This, together with the fact that the excitation spectrum does not match well with the absorbance spectrum for Ag nanocrystals in glass (Fig. 19), indicates that not the Ag nanocrystals but the Ag^+ ions cause the enhanced Er excitation. Note that in the sample that contains Ag nanocrystals, a large fraction of the Ag is still present in ionic form.

To find out what Ag^+-related energy level in the glass causes the sensitizing effect, the absorbance spectrum in Fig. 19 can be further considered. The absorbance observed for the sample without nanocrystals is several orders of magnitude higher than what would be needed to explain the Er intensity enhancement observed in Fig. 21. It could thus well be that a much weaker absorption, hidden in the main band observed in Fig. 19, is responsible for the sensitizing effect.

The absorption of Ag^+ ions in glasses is generally observed at wavelengths much shorter than the range covered by our measurements, and Ag^+ ions are therefore unlikely to take part in the excitation mechanism of Er^{3+} reported here. Several authors[57,60] have observed an absorption band in the spectral region between 300 and 450 nm in glasses containing high concentrations of Ag, and attributed it to pairs of Ag ions–atoms. It could be that such Ag pairs are at the origin of the energy transfer to Er^{3+}. It seems unlikely that the excitation takes place via the glass band edge, shifted to longer wavelengths as a result of the introduction of Ag^+ into the glass. This displacement is usually small for silver concentrations comparable to those in our samples.[57]

The sensitizer effect of Ag-related states is particularly interesting because the Ag^+ ions can also be used to define the waveguide core. Finally, let us mention that the enhancement of Er^{3+} emission by codoping with Ag is not restricted to doping by ion exchange. Samples into which silver was introduced by ion implantation also showed the broad excitation band for the PL of Er^{3+}.

5. SENSITIZED ERBIUM-DOPED ORGANIC CAGE COMPLEXES

As polymer waveguides are becoming more important, both as fibers and in thin-film configurations,[61] it is interesting to study the doping of planar polymer waveguides with Er, and to investigate if optical amplification can be achieved. Such polymer amplifiers could then be integrated into existing optical polymer devices such as splitters, switches, and multiplexers with low coupling losses.

Unfortunately, the inorganic Er salts cannot be dispersed directly into an organic matrix. To avoid this problem, the Er^{3+} ion must first be encapsulated by an organic ligand. The resulting complex can then be dispersed in a polymer film. The ligand has to be designed such that it provides enough coordination sites to bind the Er^{3+} ion and to form a stable complex.

Here, we first present the optical properties of different Er-doped polydentate hemispherands that form an overall neutral complex in which the Er^{3+} ion is encapsulated in a cagelike ligand configuration.[62] In these complexes Er can be excited directly into one of the Er^{3+} manifolds. Alternatively, it can be excited by way of the organic cage. The cage complex thus serves as a sensitizer for Er. Next, we describe how highly absorbing chromophores can be functionalized to these cage complexes. We report data for Er^{3+}, Yb^{3+}, and Nd^{3+} complexes.

A. Polydentate Cage Complex Sensitizers

Figure 22(a) shows a schematic representation of a cyclic Er^{3+} complex in which the first coordination sphere consists of either C–H bonds (cyc-H) or C–D bonds (cyc-D). An acyclic Er^{3+} complex (acyc-H), sketched in Fig. 22(b), was also studied: It is open at the top and contains two $O(CH_2)_3CH_3$ groups. This is slightly different compared with the cyclic complexes, which are closed at the top and have one $C_{18}H_{37}$ chain attached to the trivalent nitrogen atom. A three-dimensional representation of the cyclic complex is shown in Fig. 22(c). Figure 23 shows the schematic energy level diagram of the Er-doped cage complex. The complex is first excited from the singlet S_0 ground state to the singlet S_1 excited state, followed by fast relaxation to the triplet T_1 state. From there, energy transfer to the Er^{3+} $4f$ levels may take place. From these levels, rapid relaxation to the $^4I_{13/2}$ first excited state in Er^{3+} takes place. Finally, the Er^{3+} may decay to the $^4I_{15/2}$ ground manifold by the emission of a 1.54-μm photon.

After synthesis, the Er^{3+}-complex solutions were dried, mixed with KBr, and then pressed to 1-mm thick tablets with a diameter of 1.2 cm. The Er concentration was $\approx$1 wt.%. This concentration does not take into account the (unknown) amount of water that may remain in the tablets as a result of the preparation process. To exclude the effect of quenching due to OH in the host, some measurements were performed on solutions in deuterated butanol ($>$ 98%) at a complex concentration of 10^{-4} M or dimethylformamide at a concentration of 2×10^{-3} M. In all solvents acyc-H dissolved rather well, but the solutions with the cyclic complexes appeared somewhat turbid, indicating that not all the material had dissolved.

Figure 24(a) shows normalized, room-temperature PL spectra for the three complexes in KBr after excitation at 488 nm into the $^4F_{7/2}$ level (see Fig. 23). Clear Er^{3+} luminescence around 1.54 μm is observed. The FWHM of all spectra is 70 nm. This is much wider than for any other Er-doped material: Er-implanted SiO_2 (11-nm FWHM),[63] phosphosilicate glass (25-nm FWHM),[63] sodalime silicate glass (19-nm FWHM),[64] Al_2O_3 (55-nm

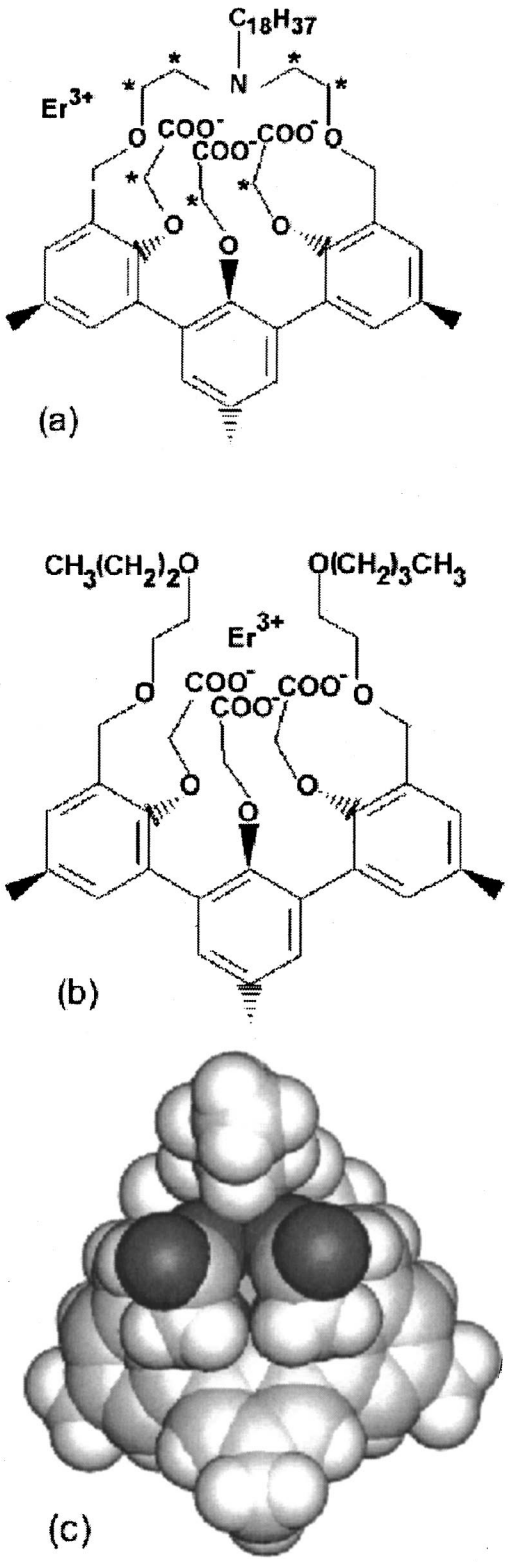

Fig. 22. Two-dimensional representation of the structure of (a) the cyclic Er^{3+} complex; asterisks represent either two H (cyc-H) or two D (cyc-D) atoms, and (b) the acyclic Er^{3+} complex (acyc-H). The outer two benzene rings lie in one plane that is tilted backward, whereas the middle benzene ring is tilted forward. In this way, a cage is constructed encapsulating the Er^{3+} ion. (c) Three-dimensional representation of the cyclic complex (cyc-H). From Slooff *et al.*, Ref. 62.

FWHM),[65] and fluorohafnate glass (64-nm FWHM).[1] Such a broad spectrum permits a wide gain bandwidth for optical amplification.

No comparison of the absolute PL intensities could be made for the three complexes, as the intensity varies over the KBr tablets (by a factor of 2–3). The spectral shapes measured for the two cyclic complexes are identical, and slightly different from that for the acyclic complex. This difference is attributed to a small difference in local environment for the two types of complexes. Figure 24(b) shows the normalized, room-temperature PL spectra for the Er^{3+} complexes in dimethylformamide. Again, the shapes of the spectra observed for cyc-H and cyc-D are similar, but slightly different compared with the spectrum of acyc-H.

Figure 25 shows the room temperature PL spectrum of acyc-H in KBr after excitation at 337 nm (pulse energy 20 μJ). The 337-nm pump light is absorbed in the tail of the absorption band of the aromatic rings of the ligand. Energy transfer to the Er^{3+} ion then leads to excitation of the Er^{3+}, resulting in the observed 1.54-μm luminescence. This is direct evidence that the aromatic rings act as a sensitizer for Er.

From extinction spectra reported in Ref. 62 the absorption cross sections for the $^4I_{15/2} \rightarrow {}^4F_{7/2}$ transition at 1.53 μm were derived: $(0.62 \pm 0.05) \times 10^{-20}\,\mathrm{cm}^2$ for acyc-H, $(1.1 \pm 0.4) \times 10^{-20}\,\mathrm{cm}^2$ for cyc-H, and $(0.93 \pm 0.05) \times 10^{-20}\,\mathrm{cm}^2$ for cyc-D. These cross sections are 1–5 times higher than the 1.5-μm cross section of Er^{3+} doped glasses[62,66] and for Er-implanted Al_2O_3.[67] This may be related to differences in average electron distribution around the Er^{3+} ion for organic complexes compared with inorganic hosts.

The luminescence lifetimes in the cyc-H complexes were found to be quite low: 0.5 μs in KBr and 0.8 μs in butanol-OD. These lifetimes are much shorter than the radiative lifetime of 4 ms estimated from the cross section spectrum. This indicates that significant quenching of the Er^{3+} luminescence takes place. From temperature-dependent measurements it was found that the large quenching is not due to a temperature-activated effect, such as, e.g., phonon-assisted decay. Selective deuteration experiments showed that coupling to vibrational states of C–H bonds was also not the main origin of the quenching. A remaining hypothesis is, then, that Er is quenched by OH groups (in the form of MeOH or water) that are coordinated to the Er^{3+} ion. OH is present in the liquids (mainly alcohols) that are used in the preparation of the Er^{3+} complexes, and in the (highly hygroscopic) solvents used for the measurements. Indeed, molecular-dynamics simulations of trivalent lanthanide complexes in solution show that one methanol or water molecule can penetrate the first coordination shell of the ion. In particular water may preferentially solvate the Er^{3+} ion.[68] It is the most potent quencher of lanthanide luminescence, and has a significantly stronger interaction with the lanthanide than, for instance, alcohols. An OH group positioned near the Er^{3+} ion will result in efficient quenching of the luminescence, because its first vibrational overtone is resonant with the $^4I_{13/2} \rightarrow {}^4I_{15/2}$ transition of Er^{3+}. Work by Ermolaev and Sveshnikova[69] shows that the rate constant for deactivation of the Er^{3+}

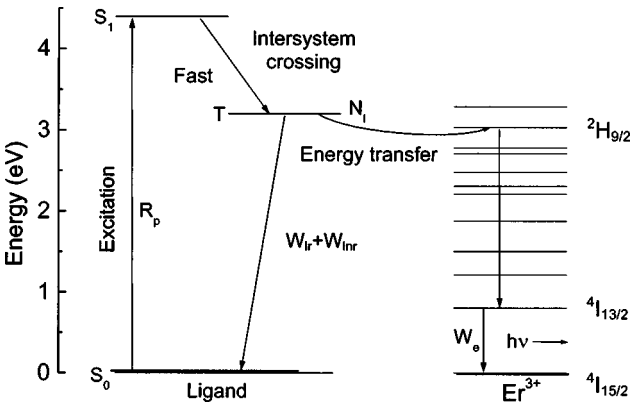

Fig. 23. Schematic diagram of the ligand-Er^{3+} system. The complex is first excited from the singlet S_0 ground state to the singlet S_1 excited state, followed by fast relaxation to the triplet T_1 state. From there, energy transfer to the Er^{3+} $4f$ levels may take place. From these levels, rapid relaxation to the $^4I_{13/2}$ first excited state in Er^{3+} takes place. Finally, the Er^{3+} may decay to the $^4I_{15/2}$ ground manifold by the emission of a 1.54 μm photon. From Slooff *et al.*, Ref. 62.

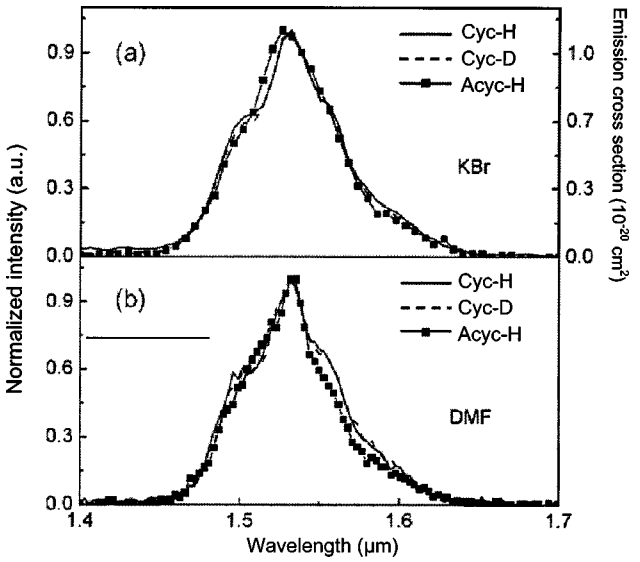

Fig. 24. Normalized room temperature PL spectra of Er^{3+} complex in (a) KBr tablets and (b) dimethylformamide, at a pump wavelength of 488 nm (power 100 mW). From Slooff *et al.*, Ref. 62.

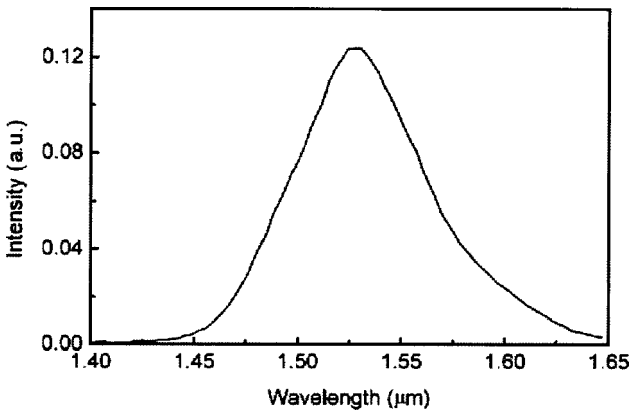

Fig. 25. Room temperature PL spectrum of acyc-H in KBr after excitation via the ligand at 337 nm (pulse energy 20 μJ). From Slooff *et al.*, Ref. 62.

excited state by way of OH groups, located at a distance of 0.22–0.25 nm is of the order of $(3-5) \times 10^8\ s^{-1}$, which is dominant over deactivation by way of C–D bonds at 0.22–0.25 nm ($k = 5 \times 10^6\ s^{-1}$).

With these short luminescence lifetimes, very high pump powers are required to invert the Er ions.[62] However, this problem can be solved by excitation of the complex by way of the aromatic part of the ligand at 287 nm. At this wavelength the absorption cross section of the ligand is $\approx 8.5 \times 10^{-18}\ cm^2$, much higher than the cross section for direct absorption of the Er^{3+} ion at 488 nm [$(1-3) \times 10^{-20}\ cm^2$]. Energy transfer from the ligand's excited state to the Er^{3+} ion then results in population of the Er^{3+} $^4I_{13/2}$ luminescent excited state. The next challenge is to engineer the ligand and to shift the excitation wavelength to the visible in order to be able to use standard semiconductor lasers or LEDs as pump sources. Alternatively, an organic sensitizer with a high absorption coefficient may be attached to the complex to further optimize the pump efficiency. This will be discussed in Subsection 5.B.

B. Sensitized Emission of Er^{3+} and other Lanthanides in Chromophore-Functionalized Complexes

The great flexibility of organic chemistry makes it possible to functionalize organic lanthanide complexes with a highly absorbing chromophore that serves as an optical antenna by which energy transfer to the lanthanide may take place. The chromophore can be selected to match the desired pump wavelength, typically in the wavelength range 500–700 nm. The energy transfer scheme in these complexes is very similar to that drawn in Fig. 23: Absorption of a photon brings the sensitizer into its singlet excited state, after which intersystem crossing populates the triplet excited state. From this state, energy transfer occurs to the complexed Ln^{3+} ion.[70]

This energy transfer is of the Dexter type.[71] Factors that determine the rate of energy transfer are (i) the spectral overlap of the normalized emission and absorption spectrum of the donor and acceptor, respectively, (ii) the distance between the donor and the acceptor, and (iii) the energy gap between the donating level of the donor and the accepting level of the Ln^{3+} ion. A representative complex with lissamine as the sensitizer is shown in Fig. 26. The distance between the center of the sensitizer—the gray part—and the Ln^{3+} ion is $\approx$1 nm. The effective average Bohr radius for the excited lissamine and the unexcited Nd^{3+} ion is $\approx$0.25 nm. In this particular example, the small spatial overlap leads to an energy transfer rate that is only 3% of the rate that would be achieved in the (idealized) case of complete coupling. Several alternative complexes were fabricated that have much better coupling.

Until now, fluorescein, erythrosine, eosin, triphenylene, porphyrin, and $Pt(PPh_3)_2$ catecholate have been shown to act as sensitizers for Er^{3+}.[72–77] Fluorescein, erythrosine, eosin, triphenylene, dansyl, lissamine, coumarin, ferrocene, Ru(bipyridine)$_3$, and a Pt(II) complex also sensitize Nd^{3+} and Yb^{3+}.[72,73,76,78] The emission spectra of

Nd^{3+}, Yb^{3+}, and Er^{3+} complexes functionalized with fluorescein are shown in Fig. 27. In these complexes the fluorescein is placed at approximately 0.6 nm from the Ln^{3+} ion.[72]

De Sa *et al.*[70] and Gonçalves e Silva *et al.*[79] derived selection rules for Förster and Dexter energy transfer to Eu^{3+} and Sm^{3+}. The selection rules for energy transfer from sensitizer to the Ln^{3+} $^{(2S+1)}\Gamma_J$ $4f$ levels are $|\Delta J| = 2, 4, 6,...$ for the dipolar and multipolar energy transfer (Förster type) and $|\Delta J| = 0, 1$ (but forbidden for $J = J' = 0$) for the electron exchange mechanism (Dexter type). It should be noted that these rules are (somewhat) relaxed by mixing from allowed transitions (e.g., $4f$–$5d$ transitions).[80] We have identified the $^4I_{13/2}$ level as the most likely level of Er^{3+} to which fluorescein, eosin, and erythrosine donate their energy.[72] With triplet state energies in the range of 15,000–16,000 cm^{-1}, this implies that the energy gap with the $^4I_{13/2}$ level of Er^{3+} is large (6,500 cm^{-1}) and consequently the energy transfer rate low. The energy transfer rate could be improved by using a sensitizer with lower triplet energy. Ideally, the triplet energy should then be 1,500–2,000 cm^{-1} above the $^4I_{13/2}$ level of Er^{3+}. This small energy gap then would prevent energy backtransfer.

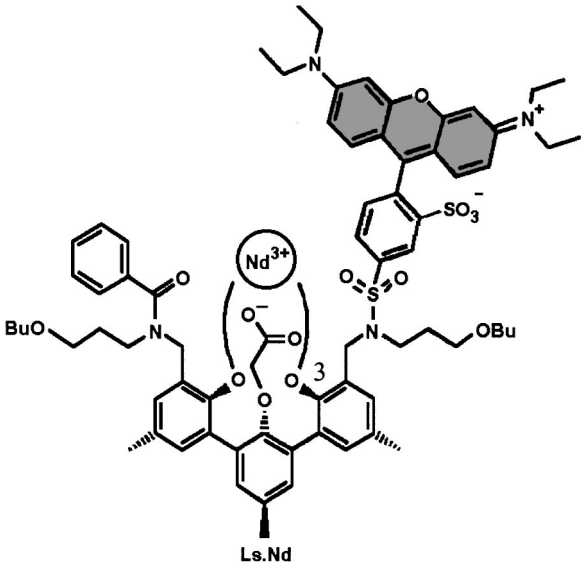

Fig. 26. Two-dimensional representation of the lissamine-Nd^{3+} complex. From Slooff *et al.*, Ref. 87.

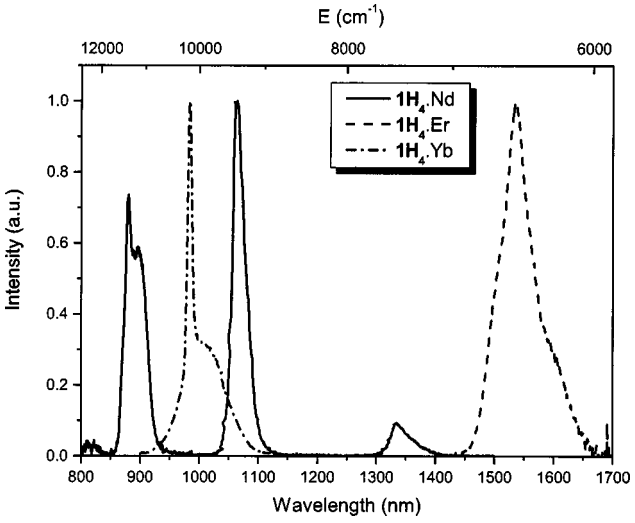

Fig. 27. Near-infrared emission spectra of Nd^{3+}-, Yb^{3+}-, and Er^{3+}-sensitized complexes similar to that shown in Fig. 26, but with a fluorescein as sensitizer, in CH_3OD (Nd^{3+} and Yb^{3+}) and in CD_3OD (Er^{3+}) solution; $\lambda_{ex} = 505$ nm. From Hebbink *et al.*, Ref. 72.

As mentioned above, typically the level from which energy transfer occurs is the first triplet excited state of the sensitizer. Some sensitizers, however, show almost exclusive energy transfer from the first singlet excited state. So far, lissamine and dansyl have shown this for the sensitized emission of Nd^{3+}.[81] As this stage it is not known if energy transfer from the first singlet excited state of the sensitizer to Er^{3+} is possible. In such a case energy transfer could also take place through Förster transfer by exciting the $^4I_{15/2} \rightarrow {}^4I_{11/2}$ transition in Er^{3+} ($\Delta J = 2$).[70,79]

In selecting a proper sensitizer for a given lanthanide ion, one would intuitively consider a sensitizer with a low fluorescence efficiency, i.e., a high intersystem crossing rate. However, as it turns out, the presence of a Ln^{3+} ion can increase the intersystem crossing quantum yield even for sensitizers that have a small intrinsic intersystem crossing yield. Sensitizers with inherent high yields of fluorescence, e.g., fluorescein, have intersystem crossing quantum efficiency larger than 90% when bound to a Ln^{3+} complex similar to that in Fig. 27.[72] Major factors in engineering the Ln^{3+}–sensitizer combination are matching the donating and accepting levels and bringing the sensitizer close to the Ln^{3+} ion. The latter can easily be done by making complexes in which the sensitizer is coordinated directly to the Ln^{3+}. We have shown this for Eu^{3+}, Nd^{3+}, Yb^{3+}, and Er^{3+} with β-diketonates as sensitizer.[82,83]

C. Lissamine-Functionalized Nd^{3+} Complexes in Polymer Waveguides

In this section we further explore the optical properties of one specific Ln^{3+}-sensitizer combination, that of a terphenyl-based Nd^{3+} complex with and without a highly absorbing lissamine antenna chromophore in the form of a Rhodamine-B derivative (termed Ls.Nd and Bz.Nd, respectively).[84] The complexes were synthesized by the procedure described in Ref. 85 (see Fig. 26). The complexes were dissolved in hexadeutero-dimethylsulfoxide (DMSO-d6) to a concentration of 10^{-2} M for Bz.Nd and 10^{-6} M for Ls.Nd, or dissolved in partially fluorinated polycarbonate[86] waveguides at a concentration of 3 wt.% (complex).

In complexes without lissamine, excitation of the Nd^{3+} ion at a wavelength of 515 nm leads to population of the $^4G_{7/2}$ level, from which it decays to the $^4F_{3/2}$ level. Decay from this level leads to the characteristic Nd^{3+} luminescence at 890, 1060, and 1340 nm due to transitions to the $^4I_{9/2}$, $^4I_{11/2}$ and $^4I_{13/2}$ levels, respectively (see Fig. 27).

Figure 28 shows the PL intensities at 1060 nm for a 10^{-2} M solution of Bz.Nd and a 10^{-6} M solution of Ls.Nd, both in DMSO-d6, at different excitation wavelengths as available from the Ar-ion laser.[87] The absorption spectrum measured for the same solutions is also included in the figure. The pump power for excitation was 60 mW

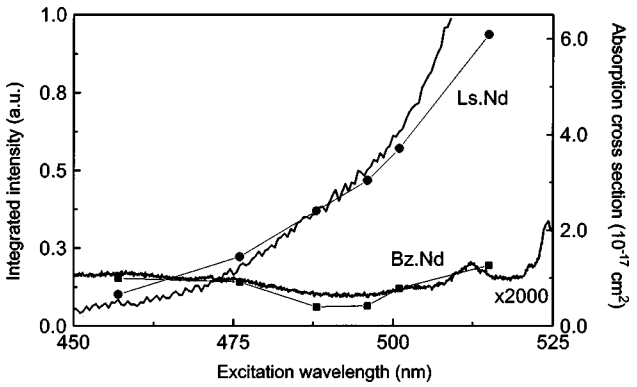

Fig. 28. PL at 1060 nm as a function of excitation wavelength for the benzoyl-Nd^{3+} complex (Bz.Nd) (10^{-6} M, squares) and the lissamine functionalized Nd^{3+} complex (Ls.Nd) (10^{-6} M, circles) in DMSO-d6 solutions. The absorption spectra of Bz.Nd and Ls.Nd are also shown (drawn curves). Note that the absorption data for the Bz.Nd solution are multiplied by a factor of 2000. From Slooff *et al.*, Ref. 87.

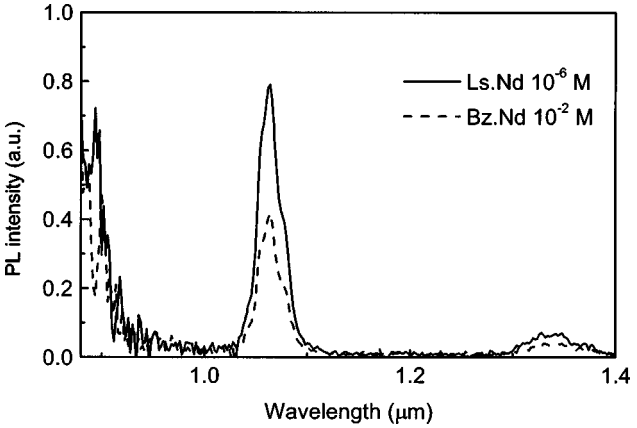

Fig. 29. PL spectra of lissamine-functionalized Nd^{3+} complex (Ls.Nd) (10^{-6} M) and the benzol-Nd^{3+} complex (10^{-6} M) in solutions. The excitation wavelength is 515 nm at a pump power of 60 mW. Note that at ≈1340 nm the spectra are multiplied by a factor of 5. From Slooff *et al.*, Ref. 87.

for all excitation wavelengths. The excitation spectrum for the complex without sensitizer (Bz.Nd) shows some structure that is roughly similar to that found in the absorption measurement, and is consistent with the absorption bands of the Nd^{3+} ion at ≈475 nm and ≈513 nm. The excitation spectrum for the complex with sensitizer (Ls.Nd) shows a completely different behavior: The 1060-nm emission intensity increases strongly with excitation wavelength, again very similar to what is found for the absorption spectrum. Given that the lissamine complex shows a broad absorption band at ≈580 nm, this clearly indicates that the excitation of Nd^{3+} at ≈500 nm takes place by way of the sensitizer. The absorption of the lissamine occurs at the xanthene unit (i.e., the gray part in the structure for Ls.Nd in Fig. 26). Note that the measured absorption cross section is in the 10^{-17} cm^2 range, which is four orders of magnitude higher than the typical Nd^{3+} intra-4*f* transition cross section.

Figure 29 shows the room-temperature PL spectra for 10^{-2}-M Bz.Nd and 10^{-6}-M Ls.Nd in DMSO-d6 as recorded under excitation at 515 nm at a pump power of 60 mW. The complexes show room-temperature PL of Nd^{3+} at 890, 1060, and 1340 nm. Although the concentration of Ls.Nd is 10^4 times lower than the concentration of Bz.Nd, the PL intensity is 2 times higher. Optical absorption measurements at 515 nm for both solutions show an almost identical absorption: 0.033 cm^{-1} for 10^{-2} M Bz.Nd and 0.031 cm^{-1} for 10^{-6} M Ls.Nd. That the sensitized complex shows higher luminescence than the complex without a sensitizer, even though the measured absorption was the same, indicates that the internal energy transfer efficiency within the sensitized complex is quite high. The factor of 2 difference can be due to the fact that upon direct excitation into the higher-lying state of the Nd^{3+} ion, the Nd^{3+} ion can also decay radiatively to the ground level (indeed, 524-nm luminescence has been observed as a result of the $^2K_{13/2} \rightarrow {}^4I_{9/2}$ transition), resulting in a lower quantum yield for the near-infrared transitions in the case of direct optical excitation of the Nd^{3+} at 515 nm. The measured luminescence lifetime at 1060 nm for the Bz.Nd complex in DMSO-d6 is 2.5 μs, while for the sensitized Ls.Nd complex it is 2.2 μs. The luminescence lifetime of Nd^{3+} in inorganic materials can be as high as 250 μs.[88] The low quantum yield in the organic complexes is attributed to quenching of the Nd^{3+} excited state by coupling to overtones of nearby C–H and O–H vibrational states.

Finally, we note that these lissamine-functionalized complexes do show significant photodegradation under optical pumping. A more detailed description of these phenomena is presented in Ref. 87. A novel and promising material that may solve this problem is a silica-based film doped with Er tris 8-hydroxyquinoline (ErQ) which is made by a solgel process.[89] Sensitized emission of Er through the hydroxyquinoline ligand in ErQ has been observed in this compound.

D. Toward an Electrically Pumped Sensitized Planar Amplifier

Recently, the Friend group at Cambridge University and we have shown 890-nm luminescence from a Nd-doped polymer under electrical excitation in a LED.[90] The active layer was a blend of poly(dioctylfluorene-cobenzothiadiazole) and a lissamine-functionalized, terphenyl-based Nd complex. It was shown that charge injection into the conducting polymer was followed by energy transfer to the sensitizer, resulting in excitation of the Nd ion. By using this concept of energy transfer from a conjugated polymer to a sensitized rare-earth complex, it becomes possible to fabricate an electrically pumped, polymer waveguide amplifier operating in the near-infrared. Note that there is no conjugated polymer known that emits at these and longer wavelengths. To have energy transfer from the polymer to the sensitizer, the sensitizer and conjugated polymer must be chosen such that the emission of the polymer overlaps the absorption spectrum of the sensitizer. More details are given in Ref. 90. Kawamura *et al.* have demonstrated similar electroluminescence for Nd-, Er-, and Yb-doped organic complexes embedded in polymer LEDs.[91]

6. COUPLED WAVEGUIDE DESIGN FOR SENSITIZED PLANAR AMPLIFIER

As shown in the previous sections, several strongly absorbing sensitizers for Er are available. One major advantage of a sensitizer is that it provides a means to pump the Er ions at alternative wavelengths for which more convenient pump sources are available. Note that a sensitizer does not increase the pump efficiency, defined as the Er excitation efficiency per absorbed pump photon. In fact, if a strongly absorbing sensitizer is added to the waveguide, the pump will be very rapidly absorbed and only a small fraction of the waveguide pumped. This was illustrated in Section 2 for the weak sensitizer Yb, and this effect will be much stronger for Si-nanocrystal- or lissamine-sensitized waveguides. For such highly absorbing sensitizers a pump geometry may be used in which the pump is projected perpendicular to the sample.

Such a geometry, however, is not always easily constructed, as it is difficult to focus the light onto a narrow waveguide; thus, an alternative design was developed that is described here.[92] In this design the pump is gradually coupled from a nonabsorbing pump guide into the adjacent amplifying guide. By gradually increasing the coupling (i.e., reducing the distance between the guides), it is even possible to maintain a constant pump power along the signal guide.

As an example we will consider a lissamine-sensitized, Nd^{3+}-doped polymer waveguide. In these complexes, 1340-nm emission of Nd is observed after excitation by the strongly absorbing lissamine sensitizer at 515 nm. If the pump power is higher than the value needed for complete population inversion of the Nd, the excess pump light is still absorbed by the lissamine, leading to a reduced pumping efficiency. Therefore, the pump power should be kept below a certain limit over the length of the waveguide.

In this example, the pump power ($\lambda = 515\,\mathrm{nm}$) is coupled through a 0.5-μm wide waveguide parallel to a 1.8-μm wide signal waveguide ($\lambda = 1340\,\mathrm{nm}$) at a spacing between the centers of the waveguide of 2 μm. Both waveguides support only the fundamental mode. In the present geometry, coupling from the signal waveguide into the pump waveguide is negligible, as the narrow pump guide does not support the 1340-nm mode.

Figure 30 shows the intensity distribution of the pump over the length of the waveguide that was calculated by use of coupled-mode theory. The input pump power was 1.0 W. The intensity decrease in the nonabsorbing pump guide is entirely due to absorption of pump light coupled into the highly absorbing signal waveguide. In the present configuration the pump power is almost completely absorbed after a distance of about 4 cm. The pump power in the signal guide as a function of the distance follows the same decreasing trend because the coupling constant is constant over the length of the waveguides. This is not visible on the scale of Fig. 30 because the coupling constant is very small. The pump power in the signal guide can be determined by integrating the data in Fig. 30 across the signal waveguide. The result is shown in Fig. 31. As can be seen, the power in the signal guide decreases from about 6 mW to almost zero over a distance of 4 cm.

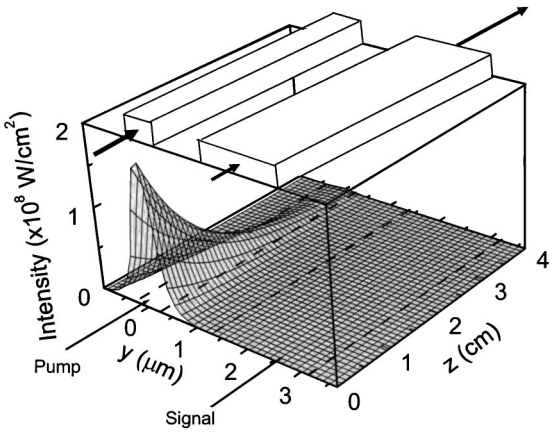

Fig. 30. Pump intensity in the waveguide structure as a function of distance z along the waveguide. From Slooff *et al.*, Ref. 92.

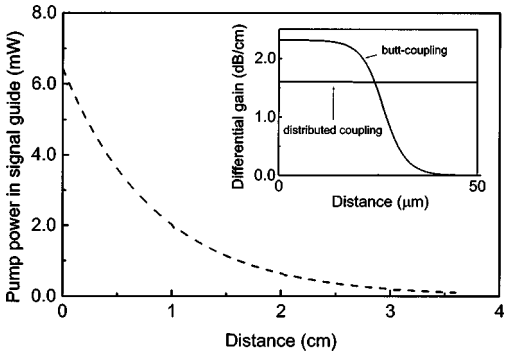

Fig. 31. Pump power in the signal guide as function of distance z in a sensitized Nd^{3+}-doped polymer waveguide. The inset shows the calculated differential gain as a function of distance along the waveguide for a coupled waveguide system and a butt-coupled waveguide. The input power in the pump waveguide is 1 W in both cases. From Slooff *et al.*, Ref. 92.

The Nd^{3+} level system can be described by a four-level system in which there is no minimum pump power required for optical gain. The differential gain along the amplifier is calculated by using the known rate equations for the Nd^{3+} level system, which are given in Ref. 92, and the pump power as a function of distance shown in Fig. 30. The result is shown in the inset of Fig. 31. Note that even with a pump power as low as 6 mW at the beginning of the signal guide, the differential gain is still reasonably high ($\approx$1.6 dB/cm). The total optical gain for this waveguide amplifier is calculated to be 1.6 dB for a 4-cm long waveguide amplifier for a waveguide with $5 \times 10^{19}\,\mathrm{Nd/cm^3}$.[92] To show the advantage of distributed coupling, the inset of Fig. 31 also includes the differential gain obtained by using conventional butt coupling at the same input pump power of 1 W. Note that all pump power is completely absorbed within the first 50 μm. The total gain for this case is only 0.005 dB.

7. COMPARING THE FOUR SENSITIZER CONCEPTS

Four sensitizing concepts have been reviewed in this article. Yb is the weakest sensitizer of the four, with an ab-

sorption cross section at 980 nm that is ≈10 times higher than that of Er at 980 nm. The relatively weak sensitization effect enables the use of Yb in waveguide geometries where pump and signal are copropagating. By a careful choice of waveguide length and Er and Yb concentration, Yb can provide enhanced gain for a given pump power. Because of their narrow absorption spectrum, Yb ions must be pumped through a laser source. The detailed nature of Ag as a sensitizer for Er needs to be explored further. The effective sensitization efficiency in Ag-doped silica glass was found to be somewhat higher than that of Yb, and occurs over a broad wavelength range.

Si nanocrystals have very broad absorption, and a 10,000-times-higher absorption cross section than Er. This enables the use of a white light source or LED as the pump. The high cross section implies that the waveguide must be pumped from the top or the side, thus requiring a novel integration design. The same is true for the organic sensitizers functionalized with Er. Organic chemistry has the great advantage of flexibility in design, so that the sensitizer absorption spectrum can be matched to the desired pump source. The main disadvantage of these organic complexes is the low internal quantum efficiency of the lanthanides. In addition, the organic cage complexes exhibit relatively strong photodegradation. Organic sensitizers may find applications in electrically pumped devices, where they play an essential role in mediating the energy transfer between the electrically conducting polymer. One way to solve the internal quenching problem of the lanthanides would be to incorporate them in an inorganic nanostructure (e.g., silica, silicate), which can then be functionalized such that it can be dissolved in an organic (polymer) matrix. Initial experiments on this concept showed promising results.[93,94] The next challenge would be to integrate an organic sensitizer into this organic–inorganic nanocomposite material in such a way that it couples to the lanthanide ion.

One important effect of the use of a sensitizer is the reduction of ESA, in particular when a broadband pump is used rather than an intense laser source. Note that for Yb as a sensitizer, typically a 980-nm pump laser is required, and this wavelength does cause ESA in Er. For the other sensitizers that have broadband absorption, the pump source may be selected such that it does not cause ESA.

To enable high gain over a short length, high Er concentrations are required. Using Si nanocrystals as a sensitizer results in a limit to the amount of the Er that can be incorporated, as the nanocrystals themselves take up a significant volume fraction. Given the observation that a single nanocrystal can excite only a single Er ion, the Er/nanocrystal ratio must be carefully engineered. One factor that may be of help here is the preliminary observation that the optical cross sections of Er in silica are enhanced by the presence of Si nanocrystals.

In terms of fabrication technology, Yb codoping typically is compatible with Er-doped glass fabrication technology. Ag is particularly attractive as a sensitizer in Ag-ion-exchanged glass in which Ag ions serve to define the waveguide core as well, thus enabling high overlap between waveguide mode and sensitizer distribution. Si nanocrystals are relatively easily made by precipitation from a supersaturated solution of Si in SiO_2 that can be made by using low-pressure chemical vapor deposition. Organic synthesis enables the fabrication of large quantities at low cost and easy integration with spin-coating technology to form polymer-based waveguides.

8. ERBIUM ITSELF AS A SENSITIZER

Finally, we note two interesting examples where Er itself can act as a sensitizer. As mentioned in Section 3, bulk semiconductors are in principle ideal sensitizers for Er, as the coupling between excitonic states in the semiconductor and the Er $4f$ electronic states is very strong. For Er in crystalline Si the coupling leads to a (unwanted) backtransfer process in which excited Er decays by the generation of an electron–hole pair in the Si crystal. This backtransfer can be used in an advantageous way to achieve infrared photodetection in Si, as we recently demonstrated.[95] In this scheme, a Si p-n junction is doped with Er ions. Infrared light incident on the device is absorbed by the Er ions, and subsequently electron–hole pairs are generated in the Si by backtransfer. Electrons and holes are then separated by the internal electric field in the junction, and thus a photocurrent can be detected. So the Er ions act as sensitizer for electronic excitations in the semiconductor crystal.

In a second example of energy transfer away from Er, the interaction between Er and Tm was studied. Tm shows broadband emission in the 1600–2100-nm wavelength range. Materials codoped with Er and Tm could thus serve as gain media in optical amplifiers with very high bandwidth. Recently, we studied Er- and Tm-codoped, silicon-rich SiO_2 in which both Er and Tm were sensitized through Si nanocrystals.[96] It was found that significant energy transfer occurred from excited Er to excited Tm, causing quenching of Er and upconversion of Tm ions into their third excited state. The upconverted Tm ions cause transitions at a wavelength slightly shorter than that of Er, thus providing yet a third band of optical amplification in Er–Tm codoped material.

9. CONCLUSIONS

In this paper, after a brief review of the sensitizing concept for the Yb–Er system, three sensitizers for erbium have been reviewed based on semiconductor nanocrystals (Si), metal ions (Ag), and organic complexes. Sensitizers serve to increase the excitation rate per incoming photon, or to permit excitation of Er at wavelengths at which Er itself shows no absorption. For the Yb–Er case it is shown with a rate-equation model that the sensitizing is effective only for well-chosen Yb and Er concentration ratios that depend critically on waveguide length and available pump power. Silicon nanocrystals have broadband absorption for wavelengths below 900 nm. They can couple to Er at a rate faster than the internal nanocrystal recombination rate, and with very high efficiency, but the number of Er ions that can be excited is limited to 1–2 per nanocrystal. Silica glass doped with Ag^+ ions also shows a strong sensitizing effect that we attribute to a Ag^+-related defect that absorbs strongly and couples to

Er^{3+}. The strongest sensitizing effect is observed at 360 nm and extends up to ≈600 nm. Finally, rare-earth-doped organic cage complexes are addressed that can be integrated with polymer technology. Er^{3+} ions can be sensitized through the aromatic ring of the polydentate cage at ≈300 nm. By attaching strongly absorbing chromophores such as lissamine, a strong sensitizing effect is found in the visible spectral range (580 nm). Finally, we address which sensitizer is most suitable for a particular application, and show two examples where Er itself serves as a sensitizer.

ACKNOWLEDGMENTS

This work is part of the research program of the Foundation for Fundamental Research on Matter (FOM) and was made possible by financial support from the Dutch Organization for the Advancement of Research (NWO), the Netherlands Technology Foundation (STW), and Symmorphix Inc. It is a great pleasure to acknowledge all coworkers who have contributed to the work described in this review article: P. G. Kik, L. H. Slooff, Ch. Strohhöfer, and A. Tip at FOM–Institute for Atomic and Molecular Physics; M. P. Oude Wolbers, S. I. Klink, G. A. Hebbink, L. Grave, B. Snellink-Ruël, L. A. Woldering, and P. G. B. Oude Alink at the University of Twente; and J. W. M. Hofstraat at Philips Research. K. de Geus is gratefully acknowledged for the careful editing of the manuscript, and we thank J. Herek for thoughtful suggestions for improvement of the manuscript.

Corresponding author A. Polman's e-mail address is polman@amolf.nl.

*Present address, University of Victoria, Canada.

REFERENCES AND NOTES

1. W. J. Miniscalco, "Erbium-doped glasses for fiber amplifiers at 1500 nm," J. Lightwave Technol. **9**, 234–250 (1991).
2. E. Desurvire, *Erbium-Doped Fiber Amplifiers: Principles and Applications* (Wiley, New York, 1994).
3. S. Hüffner, *Optical Spectra of Transparent Rare-Earth Compounds* (Academic, New York, 1978).
4. G. N. van den Hoven, A. Polman, C. van Dam, J. W. M. van Uffelen, and M. K. Smit, "Net optical gain at 1.53 μm in Er-doped Al_2O_3 waveguides on silicon," Appl. Phys. Lett. **68**, 1886–1888 (1996).
5. M. K. Smit, "Integrated optics in silicon-based aluminium oxide," Ph.D. thesis (Delft University of Technology, Delft, The Netherlands, 1991).
6. R. N. Ghosh, J. Shmulovich, C. F. Kane, M. R. X. de Barros, G. Nykolak, A. J. Bruce, and P. C. Becker, "8-mV threshold Er^{3+}-doped planar waveguide amplifier," IEEE Photon. Technol. Lett. **8**, 518–520 (1996).
7. T. Kitagawa, K. Hattori, K. Shuto, M. Yasu, M. Kobayashi, and M. Horiguchi, "Amplification in erbium-doped silica-based planar lightwave circuits," Electron. Lett. **28**, 1818–1819 (1992).
8. Y. C. Yan, A. J. Faber, H. de Waal, P. G. Kik, and A. Polman, "Erbium-doped phosphate glass waveguide on silicon with 4.1 dB/cm gain at 1.535 μm," Appl. Phys. Lett. **71**, 2922–2924 (1997).
9. G. N. van den Hoven, E. Snoeks, A. Polman, C. van Dam, J. W. M. van Uffelen, and M. K. Smit, "Upconversion in Er-implanted Al_2O_3 waveguides," J. Appl. Phys. **79**, 1258–1266 (1996).
10. P. G. Kik and A. Polman, "Erbium-doped optical-waveguide amplifiers in silicon," MRS Bull. **23**, 48–54 (1998).
11. P. G. Kik and A. Polman, "Cooperative upconversion as the gain-limiting factor in Er-doped miniature Al_2O_3 optical waveguide amplifiers," J. Appl. Phys. **93**, 5008–5012 (2003).
12. M. P. Hehlen, N. J. Cockroft, T. R. Gosnell, and A. J. Bruce, "Spectroscopic properties of Er^{3+}- and Yb^{3+}-doped soda-lime silicate and aluminosilicate glasses," Phys. Rev. B **56**, 9302–9318 (1997).
13. E. Cantelar, J. A. Munoz, J. A. Sanz-García, and F. Cussó, "Yb^{3+} to Er^{3+} energy transfer in $LiNbO_3$," J. Phys. Condens. Matter **10**, 8893–8903 (1998).
14. S. Taccheo, P. Laporta, and C. Svelto, "Wide tuneable single-frequency erbium–ytterbium phosphate glass laser," Appl. Phys. Lett. **68**, 2621–2624 (1996).
15. D. L. Veasey, D. S. Funk, P. M. Peters, N. A. Sanford, G. E. Obarski, N. Fontaine, M. Young, A. P. Peskin, W.-C. Liu, S. N. Houde-Walter, and J. S. Hayden, "Yb/Er-codoped and Yb-doped waveguide lasers in phosphate glass," J. Non-Cryst. Solids **263&264**, 369–381 (2000).
16. J. E. Townsend, W. L. Barnes, K. P. Jedrzejewski, and S. G. Grubb, "Yb^{3+}-sensitized, Er^{3+}-doped silica optical fibre with ultrahigh transfer efficiency and gain," Electron. Lett. **27**, 1958–1959 (1991).
17. J. Nilsson, S. U. Alam, J. A. Alvarez-Chavez, P. W. Turner, W. A. Clarkson, and A. B. Grudinin, "High-power and tunable operation of erbium–ytterbium-codoped, cladding-pumped fiber lasers," IEEE J. Quantum Electron. **37**, 987–994 (2003).
18. C. Strohhöfer and A. Polman, "Absorption and emission spectroscopy in Er^{3+}–Yb^{3+}-doped aluminum oxide waveguides," Opt. Mater. (Amsterdam, Neth.) **21**, 705–712 (2003).
19. M. E. Fermann, D. C. Hanna, D. P. Shepherd, P. J. Suni, and J. E. Townsend, "Efficient operation of an Yb-sensitized Er fibre laser at 1.56 μm," Electron. Lett. **24**, 1135–1136 (1988).
20. J. E. Roman, P. Camy, M. Hempstead, W. S. Brocklesby, S. Nouh, A. Beguin, S. Lerminiaux, and J. S. Wilkinson, "Ion-exchanged Er/Yb waveguide laser at 1.5 μm pumped by laser diode," Electron. Lett. **31**, 1345–1346 (1995).
21. C. Strohhöfer and A. Polman, "Relationship between gain and Yb^{3+} concentration in Er^{3+}–Yb^{3+}-doped waveguide amplifiers," J. Appl. Phys. **90**, 4314–4320 (2001).
22. See, e.g., A. Polman, "Erbium-implanted thin-film photonic materials," J. Appl. Phys. **82**, 1–39 (1997), and references therein.
23. S. Coffa, G. Franzó, F. Priolo, A. Polman, and R. Serna, "Temperature dependence and quenching processes of the intra-4f luminescence of Er in crystalline Si," Phys. Rev. B **49**, 16313–16320 (1994).
24. P. N. Favennec, H. L'Haridon, D. Moutonnet, M. Salvi, and M. Gauneau, "Optical activation of Er^{3+} implanted in silicon by oxygen impurities," J. Appl. Phys. **29**, 524–526 (1990).
25. N. Hamelin, P. G. Kik, J. F. Suyver, K. Kikoin, A. Polman, A. Schönecker, and F. W. Saris, "Energy backtransfer and infrared photoresponse in erbium-doped, silicon p-n diodes," J. Appl. Phys. **88**, 5381–5387 (2000).
26. T. Kimura, A. Yokoi, H. Horiguchi, R. Saito, T. Ikoma, and A. Sato, "Electrochemical Er doping of porous silicon and its room-temperature luminescence at ≈1.54 μm," Appl. Phys. Lett. **65**, 983–985 (1994).
27. Jung H. Shin, G. N. van den Hoven, and A. Polman, "Direct experimental evidence for trap-state mediated excitation of Er^{3+} in silicon," Appl. Phys. Lett. **67**, 377–379 (1995).
28. S. Lombardo, S. U. Campisano, G. N. van den Hoven, A. Cacciato, and A. Polman, "Room-temperature luminescence from Er-implanted semi-insulating polycrystalline silicon," Appl. Phys. Lett. **63**, 1942–1944 (1993).
29. S. Lombardo, S. U. Campisano, G. N. van den Hoven, and

A. Polman, "Erbium in oxygen-doped silicon: electroluminescence," J. Appl. Phys. **77**, 6504–6510 (1995).
30. S. Lombardo, S. U. Campisano, G. N. van den Hoven, and A. Polman, "Room-temperature luminescence in semi-insulating polycrystalline silicon implanted with Er," Nucl. Instrum. Methods Phys. Res. B **96**, 378–381 (1995).
31. G. N. van den Hoven, Jung H. Shin, A. Polman, S. Lombardo, and S. U. Campisano, "Erbium in oxygen-doped silicon: optical excitation," J. Appl. Phys. **78**, 2642–2650 (1995).
32. M. Fujii, M. Yoshida, Y. Kanzawa, S. Hayashi, and K. Yamamoto, "1.54-μm photoluminescence of Er^{3+} doped into SiO_2 films containing Si nanocrystals: evidence for energy transfer from Si nanocrystals to Er^{3+}," Appl. Phys. Lett. **71**, 1198–1200 (1997).
33. M. Fujii, M. Yoshida, S. Hayashi, and K. Yamamoto, "Photoluminescence from SiO_2 films containing Si nanocrystals and Er: effects of nanocrystalline size on the photoluminescence efficiency of Er^{3+}," J. Appl. Phys. **84**, 4525–4531 (1998).
34. J. St. John, J. L. Coffer, Y. Chen, and R. F. Pinizzotto, "Synthesis and characterization of discrete luminescent erbium-doped silicon nanocrystals," J. Am. Chem. Soc. **121**, 1888–1892 (1998).
35. C. E. Chryssou, A. J. Kenyon, T. S. Iwayama, C. W. Pitt, and D. E. Hole, "Evidence of energy coupling between Si nanocrystals and Er^{3+} in ion-implanted silica thin films," Appl. Phys. Lett. **75**, 2011–3013 (1999).
36. G. Franzò, V. Vinciguerra, and F. Priolo, "The excitation mechanism of rare-earth ions in silicon nanocrystals," Appl. Phys. A **69**, 3–12 (1999).
37. P. G. Kik, M. L. Brongersma, and A. Polman, "Strong exciton-erbium coupling in Si-nanocrystal-doped SiO_2," Appl. Phys. Lett. **76**, 2325–2327 (2000).
38. P. G. Kik and A. Polman, "Exciton–erbium interactions in Si-nanocrystal-doped SiO_2," J. Appl. Phys. **88**, 1992–1998 (2000).
39. P. G. Kik and A. Polman, "Gain limiting processes in Er-doped, Si-nanocrystal waveguides in SiO_2," J. Appl. Phys. **91**, 534–536 (2002).
40. C. Delerue, G. Allan, and M. Lannoo, "Theoretical aspects of the luminescence of porous silicon," Phys. Rev. B **48**, 11024–11036 (1993).
41. J. Valenta, R. T. Juhasz, and J. Linnros, "Photoluminescence spectroscopy of single silicon quantum dots," Appl. Phys. Lett. **80**, 1070–1072 (2002).
42. P. G. Kik, "Energy transfer in erbium-doped optical waveguides based on silicon," Ph.D. thesis (FOM-Institute for Atomic and Molecular Physics, Amsterdam, The Netherlands, 2000).
43. D. Kovalev, J. Diener, H. Heckler, G. Polisski, N. Künzner, and F. Koch, "Optical absorption cross sections of Si nanocrystals," Phys. Rev. B **61**, 4485–4487 (2000).
44. M. L. Brongersma, P. G. Kik, A. Polman, K. S. Min, and H. A. Atwater, "Size-dependent electron–hole exchange interaction in Si nanocrystals," Appl. Phys. Lett. **76**, 351–353 (2000).
45. We assume that the nanocrystal absorption cross section and spontaneous emission lifetime are not affected by the presence of Er.
46. F. Auzel, in *Radiationless Processes*, B. DiBartolo, ed. (Plenum, New York, 1980).
47. F. Priolo, G. Franzò, S. Coffa, and A. Carnera, "Excitation and nonradiative de-excitation processes of Er^{3+} in crystalline Si," Phys. Rev. B **57**, 4443–4455 (1998).
48. K. S. Min, K. V. Shcheglov, C. M. Yang, H. A. Atwater, M. L. Brongersma, and A. Polman, "Defect-related versus excitonic visible light emission from ion-beam-synthesized Si nanocrystals in SiO_2," Appl. Phys. Lett. **69**, 2033–2035 (1996).
49. G. Franzó, D. Pacifici, V. Vinciguerra, F. Priolo, and F. Iacona, "Er^{3+} ions–Si nanocrystal interactions and their effects on the luminescence properties," Appl. Phys. Lett. **76**, 2167–2169 (2000).
50. H. S. Han, S. Y. Seo, and J. H. Shin, "Optical gain at 1.54 μm in erbium-doped silicon nanocluster sensitized waveguide," Appl. Phys. Lett. **79**, 4568–4570 (2001).
51. D. Pacifici, G. Franzò, F. Priolo, F. Iacona, and L. Dal Negro, "Modeling and perspectives of the Si nanocrystals–Er interaction for optical amplification," Phys. Rev. B **67**, 245301 (2003).
52. D. E. McCumber, "Einstein relations connecting broadband emission and absorption spectra," Phys. Rev. A **136**, 954–957 (1964).
53. W. J. Miniscalco and R. S. Quimby, "General procedure for the analysis of Er^{3+} cross sections," Opt. Lett. **16**, 258–260 (1991).
54. Hak-Seung Han, Se-Young Seo, Jung H. Shin, and Namkyoo Park, "Coefficient determination related to optical gain in erbium-doped, silicon-rich silicon oxide waveguide amplifier," Appl. Phys. Lett. **81**, 3720–3722 (2002).
55. C. Strohhöfer and A. Polman, "Silver as a sensitizer for erbium," Appl. Phys. Lett. **81**, 1414–1416 (2002).
56. R. V. Ramaswamy and R. Srivistava, "Ion-exchanged glass waveguides: a review," J. Lightwave Technol. **6**, 984–1000 (1988).
57. M. Mesnaoui, M. Maazaz, C. Parent, B. Tanguy, and G. LeFlem, "Spectroscopic properties of Ag^+ ions in phosphate glasses of $NaPO_3$–$AgPO_3$ system," Eur. J. Solid State Inorg. Chem. **29**, 1001–1013 (1992).
58. A. Meijerink, M. M. E. van Heek, and G. Blasse, "Luminescence of Ag^+ in crystalline and glassy SrB_4O_7," J. Phys. Chem. Solids **54**, 901–906 (1993).
59. D. M. Peters, C. Strohhöfer, M. L. Brongersma, J. van der Elsken, and A. Polman, "Formation mechanism of silver nanocrystals made by ion irradiation of $Na^+ \leftrightarrow Ag^+$ ion-exchanged sodalime silicate glass," Nucl. Instrum. Methods Phys. Res. B **168**, 237–244 (2000).
60. M. A. Villegas, J. M. Fernandez Navarro, S. E. Paje, and J. Llopis, "Optical spectroscopy of a soda lime glass exchanged with silver," Phys. Chem. Glasses **37**, 248–253 (1996).
61. B. Booth, in *Polymers for Lightwave and Integrated Optics*, L. A. Hornak, ed. (Dekker, New York, 1992).
62. L. H. Slooff, A. Polman, M. P. Oude Wolbers, F. C. J. M. van Veggel, D. Reinhoudt, and J. W. Hofstraat, "Optical properties of erbium-doped organic polydentate cage complexes," J. Appl. Phys. **83**, 497–503 (1998).
63. A. Polman, D. C. Jacobson, D. J. Eaglesham, R. C. Kistler, and J. M. Poate, "Optical doping of waveguide materials by MeV Er implantation," J. Appl. Phys. **70**, 3778–3784 (1991).
64. E. Snoeks, G. N. van den Hoven, and A. Polman, "Optical doping of soda-lime-silicate glass with erbium by ion implantation," J. Appl. Phys. **73**, 8179–8183 (1993).
65. G. N. van den Hoven, E. Snoeks, A. Polman, J. W. M. van Uffelen, Y. S. Oei, and M. K. Smit, "Photoluminescence characterization of Er-implanted Al_2O_3 films," Appl. Phys. Lett. **62**, 3065–3067 (1993).
66. J. N. Sandoe, P. H. Sarkies, and S. Parke, "Variation of Er^{3+} cross section for stimulated emission with glass composition," J. Phys. D **5**, 1788–1799 (1972).
67. G. N. van den Hoven, J. A. van der Elsken, A. Polman, C. van Dam, J. W. M. van Uffelen, and M. K. Smit, "Absorption and emission cross sections of Er^{3+} in Al_2O_3 slab waveguides," Appl. Opt. **36**, 3338–3341 (1997).
68. M. P. Oude Wolbers, "Lanthanide ion complexes and their luminescence properties," Ph.D. thesis (University of Twente, Enschede, The Netherlands, 1997).
69. V. L. Ermolaev and E. B. Sveshnikova, "The application of luminescence-kinetic methods in the study of the formation of lanthanide ion complexes in solution," Russ. Chem. Rev. **63**, 905–922 (1994).
70. G. F. De Sa, O. L. Malta, C. de Mello Donega, A. M. Simas, R. L. Longo, P. A. Santa-Cruz, and E. F. da Silva, Jr., "Spectroscopic properties and design of highly luminescent lanthanide coordination complexes," Coord. Chem. Rev. **196**, 165–195 (2000).
71. D. L. Dexter, "A theory of sensitized luminescence in solids," J. Chem. Phys. **21**, 836–850 (1953).

72. G. A. Hebbink, L. Grave, L. A. Woldering, D. N. Reinhoudt, and F. C. J. M. van Veggel, "Unexpected sensitization efficiency of the near-infrared Nd^{3+}, Er^{3+}, and Yb^{3+} emission by fluorescein compared to eosin and erythrosin," J. Phys. Chem. A **107**, 2483–2491 (2003), and references cited.
73. S. I. Klink, L. Grave, M. H. V. Werts, F. A. J. Geurts, J. W. Hofstraat, D. N. Reinhoudt, and F. C. J. M. van Veggel, "A systematic study of the photophysical processes in polydentate triphenylene-functionalized Eu^{3+}, Tb^{3+}, Nd^{3+}, Yb^{3+}, and Er^{3+} complexes," J. Phys. Chem. A **104**, 5457–5468 (2000).
74. M. P. Oude Wolbers, F. C. J. M. van Veggel, F. G. A. Peters, E. S. E. van Beelen, J. W. Hofstraat, F. A. J. Geurts, and D. N. Reinhoudt, "Sensitized near-infrared emission from Nd^{3+} and Er^{3+} complexes of fluorescein-bearing calix[4]arene cages," Chem.-Eur. J. **4**, 772–780 (1998).
75. N. M. Shavaleev, L. P. Moorcraft, S. J. A. Pope, Z. R. Bell, S. Faulkner, and M. D. Ward, "Sensitised near-infrared emission from lanthanides using a covalently attached Pt(II) fragment as an antenna group," Chem. Commun. (Cambridge) **10**, 1134–1135 (2003).
76. M. H. V. Werts, J. W. Verhoeven, and J. W. Hofstraat, "Efficient visible light sensitisation of water-soluble near-infrared luminescent lanthanide complexes," J. Chem. Soc., Perkin Trans. 2 **3**, 433–440 (2000).
77. M. H. V. Werts, J. W. Hofstraat, F. A. J. Geurts, and J. W. Verhoeven, "Fluorescein and eosin as sensitizing chromophores in near-infrared luminescent ytterbium(III), neodymium(III) and erbium(III) chelates," Chem. Phys. Lett. **276**, 196–201 (1997).
78. S. I. Klink, H. Keizer, and F. C. J. M. van Veggel, "Organo-d-metal complexes as new class of photosensitizers for near-infrared lanthanide emission," Angew. Chem., Int. Ed. **39**, 4319–4321 (2000).
79. F. R. Gonçalves e Silva, O. L. Malta, C. Reinhard, H. U. Güdel, C. Piguet, J. E. Moser, and J.-C. G. Bünzli, "Visible and near-infrared luminescence of lanthanide-containing, dimetallic, triple-stranded helicates: energy transfer mechanisms in the Sm^{III} and Yb^{III} molecular edifices," J. Phys. Chem. A **106**, 1670–1677 (2002).
80. G. Blasse and B. C. Grabmaier, *Luminescent Materials* (Springer-Verlag, Berlin, 1994).
81. G. A. Hebbink, S. I. Klink, L. Grave, P. G. B. Oude Alink, and F. C. J. M. van Veggel, "Singlet energy transfer as the main pathway in the sensitization of near-infrared Nd^{3+} luminescence by dansyl and lissamine dyes," ChemPhysChem **3**, 1014–1018 (2002), and references cited therein.
82. G. A. Hebbink, S. I. Klink, P. G. B. Oude Alink, and F. C. J. M. van Veggel, "Visible and near-infrared light emitting calix[4]arene-based ternary lanthanide complexes," Inorg. Chim. Acta **317**, 114–120 (2001). Erratum, **323**, 171 (2001).
83. S. I. Klink, G. A. Hebbink, L. Grave, P. G. B. Oude Alink, F. C. J. M. van Veggel, and M. H. V. Werts, "Synergistic complexation of Eu^{3+} by a polydentate ligand and a bidentate antenna to obtain ternary complexes with high luminescence quantum yields," J. Phys. Chem. A **106**, 3681–3689 (2002).
84. I. B. Berlman, *Handbook of Fluorescence Spectra of Aromatic Molecules* (Academic, New York, 1971).
85. S. I. Klink, G. A. Hebbink, L. Grave, F. C. J. M. van Veggel, D. N. Reinhoudt, L. H. Slooff, A. Polman, and J. W. Hofstraat, "Sensitized near-infrared luminescence from polydentate, triphenylene-functionalized Nd^{3+}, Yb^{3+}, and Er^{3+} complexes," J. Appl. Phys. **86**, 1181–1185 (1999).
86. R. H. Woudenberg and T. O. Boonstra, "Polymers comprising a fluorinated carbonate moiety," International patent, deposited September 3, 1998, WO 9838237.
87. L. H. Slooff, A. Polman, S. I. Klink, L. Grave, F. C. J. M. van Veggel, and J. W. Hofstraat, "Concentration effects in the photodegradation of lissamine-functionalized neodymium complexes in polymer waveguides," J. Opt. Soc. Am. B **18**, 1690–1694 (2001).
88. M. J. Weber, "Radiative and multiphonon relaxation of rare-earth ions in Y_2O_3," Phys. Rev. **171**, 283–291 (1968).
89. O. H. Park, S. Y. Seo, B. S. Bae, and J. H. Shin, "Indirect excitation of Er^{3+} in solgel hybrid films doped with an erbium complex," Appl. Phys. Lett. **82**, 2787–2789 (2003).
90. L. H. Slooff, A. Polman, F. Cacialli, R. H. Friend, G. A. Hebbink, F. C. J. M. van Veggel, and D. N. Reinhoudt, "Near-infrared electroluminescence of polymer light-emitting diodes doped with a lissamine-sensitized Nd^{3+} complex," Appl. Phys. Lett. **78**, 2122–2124 (2001).
91. Y. Kawamura, Y. Wada, and S. Yanagida, "Near-infrared photoluminescence and electroluminescence of neodymium(III), erbium(III) and ytterbium (III) complexes," J. Appl. Phys. **40**, 350–356 (2001).
92. L. H. Slooff, P. G. Kik, A. Tip, and A. Polman, "Pumping planar waveguide amplifiers using a coupled waveguide system," J. Lightwave Technol. **19**, 1740–1744 (2001).
93. G. A. Hebbink, J. W. Stouwdam, D. N. Reinhoudt, and F. C. J. M. van Veggel, "Lanthanide(III)-doped nanoparticles that emit in the near-infrared," Adv. Mater. (Weinheim, Ger.) **14**, 1147–1150 (2002).
94. J. W. Stouwdam and F. C. J. M. van Veggel, "Near-infrared emission of redispersible Er^{3+}-, Nd^{3+}-, and Ho^{3+}-doped LaF_3 nanoparticles," Nano Lett. **2**, 733–737 (2002).
95. P. G. Kik, A. Polman, S. Libertino, and S. Coffa, "Design and performance of an erbium-doped silicon waveguide detector operating at 1.5 μm," J. Lightwave Technol. **20**, 862–867 (2002).
96. S.-Y. Se, J. H. Shin, B.-S. Bae, N. Park, J. J. Penninkhof, and A. Polman, "Erbium–thulium interaction in broadband infrared luminescent silicon-rich silicon oxide," Appl. Phys. Lett. **82**, 3445–3447 (2003).